synchronous with the RSSL, the high energy coefficient values of wavelet analysis would be expected to distribute along the time-frequency relationship of the RSSL. Actually, the photocurrent response under voltage clamp followed the oscillatory change of light power density in a wide frequency range during RSSL (Figure 4D). On the other hand, the membrane potential response under current clamp response did not well follow the oscillatory change of light power density at a high-frequency region (Figure 4E). Rather, the energy coefficient value was relatively high at two time windows, one at the onset of slow depolarization and the other synchronized to the RSSL at 5–10 Hz. The robustness was also evaluated by the averaged current-clamp response (Figure 4C, *Vav*). It peaked at 1.2 s from the onset, which corresponded to 6.3 Hz. The frequency evoking robust firing of L5 pyramidal neurons was on average 6.1 ± 1.0 Hz ($n = 11$ neurons).

The ChR2-expressing neurons were shown previously to be activated by blue light even *in vivo* [10–20]. To examine whether ChRGR-expressing neurons are able to be activated *in vivo*, the local field potential (LFP) was recorded from the motor-cortical region close to the site where the Sindbis pseudovirion vectors were injected. The green LED light was focused on this site and reached the injected site through the dura mater (Figure 5A). The illumination to the contralateral non-injected site was used as a control (Figure 5B). The opto-current-clamp by RSSL evoked some LFP responses in the cortex. It also evoked electromyogram (EMG) responses in the contralateral lower limb muscles where the topographic projections of activated cortical neurons were expected. Each LFP response consisted of either positive-to-negative or negative-to-positive biphasic waves reminiscent of the population spikes of neurons. Sometimes, these LFP waves were accompanied by EMG waves. To find the frequency preferences, the wavelet analysis was applied to the LFP recordings. The frequency preference of the light-evoked responses was shown to be at 3–10 Hz (Figure 5C). Some LFP responses were evoked in-phase during the RSSL, whereas they were frequently evoked out-phase during the dark period. The RSSL also enhanced both the in-phase and out-phase responses of EMG (Figure 5D). In each animal the power spectrum was analyzed for the LFP responses (Figure 5E). In summary, the RSSL to the cortex enhanced the LFP activity preferentially at 3–10 Hz (Figure 5F).

When a neuron is repetitively fired, the expression of some immediate early gene products such as Arc, c-Fos and Zif268 are enhanced through Ca^{2+}-dependent mechanisms [29,30,31]. The expression of c-Fos was immunohistochemically identified after repetitive RSSL tests. Some of the ChRGR-expressing neurons also expressed c-Fos at a relatively high level but others did not (Figure 6A–6C and Figure S5). The expression of c-Fos was also enhanced distinctively in the cells that did not express ChRGR.

Discussion

When some of the transmembrane helixes of ChR2 was replaced by the counterparts of ChR1 and produced chimera channelrhodopsins, the exchange distinctively affected photocurrent properties such as the wavelength sensitivity, conductance, desensitization and ON-OFF kinetics [23]. For example, if a chimera channelrhodopsin consists of the first to fifth transmembrane helixes from ChR2 and the sixth to seventh helixes from ChR1, the photocurrent was enhanced in whole-cell conductance. On the other hand, by further replacement of the sixth transmembrane domain ("*f*"-to-"*F*" replacement) reduced the effective conductance to as small as that of ChR1. It is thus predicted that the domain "*F/f*" is involved in the conductance; high with "*f*" and low with "*F*". In the present study we did the reverse experiment, that is, replaced "*F*" of ChR1 with its counterpart from ChR2, and produced a chimera, ChR1-*f*. When expressed in HEK293 cells, this replacement enhanced the effective conductance without changing the reversal potential and the action spectrum. It is, thus, suggested that the "*F/f*" segment is one of the molecular determinants of photocurrent conductance by either regulating the expression of the molecule to the plasma membrane or regulating the ion flux per a molecule.

The seventh transmembrane domain has been suggested to be involved in the color tuning of channelrhodopsins [23]. Actually, the "G"-to-"g" replacement definitely blue-shifted the action spectrum of ChR1. This was also the same in the present study using ChR1-*f*. We further subdivided the "*G/g*" domain into two subdomains; the N-terminal 20 amino acids before the retinal-binding Lys ("G_1/g_1") and the C-terminal 49 amino acids after it ("G_2/g_2"). We found the "G_1"-to-"g_1" replacement blue-shifted the action spectrum, whereas the "G_2"-to-"g_2" replacement had no effect. These results clearly suggest that the "G_1/g_1" subdomain is one of the molecular determinants involved in the wavelength sensitivity.

When expressed in HEK293 cells, the photocurrent amplitude of ChR1-*fg*$_2$ (ChRGR) was relatively large in response to the green light if compared to that of ChR2 or ChR2-H134R (Figure S1). Therefore, it is the first practical optogenetic molecule with the ChR1 backbone. It was also preferentially sensitive to green light as one of the *Volvox*-derived channelrhodopsins (VChR1). Its average photocurrent evoked by 520 nm light was even larger than that of VChR1 probably because of its efficient membrane expression. The ON and OFF kinetics of ChRGR photocurrent was as fast as other ChR variants with fast photocurrent kinetics [23,32] and even faster than ChR2 or ChR2-H134R [9,14,22] (Figure S6). Remarkably, the ChRGR photocurrent was small in the desensitization and was even smaller than ChR1. It was also rapid in the recovery from desensitization. Its recovery time constant was 1.3 s at room temperature (27–30°C), which was smaller than the corresponding value of ChR1, ChR2 or ChR2-H134R (3–20 s) (Figure S6) [14,21,22,33]. These kinetic properties of ChRGR appeared to be optimal for optogenetic injection of the patterned current into a neuron (opto-current clamp). Similar to ChR1 [21], the ChRGR was sensitive to pH (Figure S7). The reversal potential was pH-dependent and was positively shifted with the reduction of pH. The τ_{OFF} was also pH-dependent although τ_{ON} and desensitization were not. Therefore, the fast kinetics of ChRGR appears to be optimized at pH 7.4.

In our experiments with the L5 pyramidal neurons the ChRGR molecules were not detectable in the spines within twelve hours after transfection although they distributed to the distal end of tufted dendrites. It is possible that it would take additional hours for the molecules to distribute in spines. Alternatively, the molecules might have some regional preferences. In either case it may be, the green light should depolarized the distal dendritic region to a certain level which is a function of the regional density of the ChRGR, the light power density at the region and the local input resistance. Since ChRGR was also distributed in the axonal membrane, the effects of simultaneous depolarization of a region including soma, dendrites and axon were investigated by the opto-current clamp of L5 pyramidal neurons. Our results suggested that an individual neuron has its unique firing frequency where the probability of action potential generation is expected to be highest [34]. This frequency was 3–10 Hz when a square light pulse was applied. The robust firing time window of RSSL also corresponded to this frequency band.

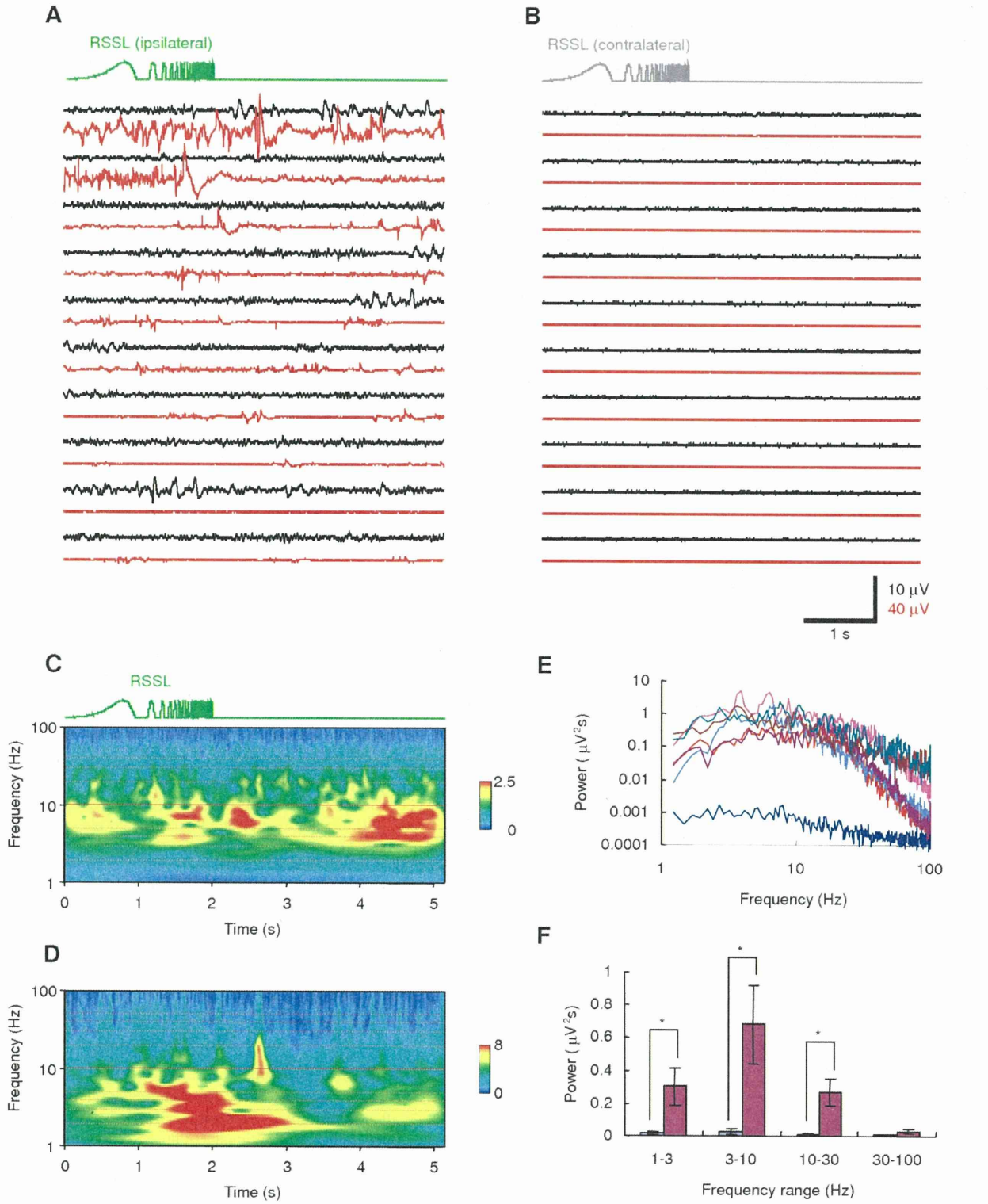

Figure 5. Opto-current clamp of the cortical network in living mice. A. The trial-to-trial responses of LFP (black lines) and EMG (red lines) under opto-current clamp by the RSSL. **B**. Control LFP and EMG traces by the RSSL on the contralateral cortex. **C**. Wavelet analysis of the LFP. **D**. Wavelet analysis of the EMG. **E**. Power spectra of opto-current-clamp responses of LFP from each animal. **F**. Summary of the LFP power spectrum analysis: control (contralateral RSSL, blue columns, left) and test (ipsilateral RSSL, crimson column, right). Asterisks indicate statistical significances ($P<0.05$, Wilcoxon signed-ranks test).
doi:10.1371/journal.pone.0012893.g005

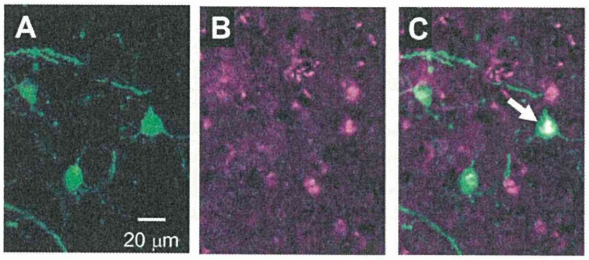

Figure 6. Spreading activity. A–C. The expression of c-Fos in the cortical neurons after a series of experiments; ChRGR-Venus (A), anti-c-Fos immunoreactivity (B) and merge (C). The white arrow indicates the ChRGR-expressing L5 pyramidal neuron which also expressed c-Fos at a relatively high level.
doi:10.1371/journal.pone.0012893.g006

When the motor cortex was exposed to the light, it was expected that the neurons in the superficial layers would be depolarized to fire directly (Figure 7A). This is consistent with our finding that some of the ChRGR-expressing neurons in these layers were also immunoreactive to anti-c-Fos. Although these neurons would fire asynchronously during RSSL and consist of both excitatory and inhibitory traits [35,36], their transmissions would be integrated in the major output neurons [37]. It was also expected that light would depolarize directly the tufted apical dendrites of a ChRGR-expressing L5 pyramidal neuron (Figure 7B). The probability of evoking action potentials would be enhanced during the depolarizing phase of the light-evoked membrane oscillation because of the asynchronous bombardments from intrinsic synaptic inputs [38]. Light-evoked depolarization also facilitates the dendrite to evoke action potentials that are dependent on either Ca^{2+} channels or NMDA receptors [39]. Consistent with this notion, some of the ChRGR-expressing L5 pyramidal neurons were also immunoreactive to anti-c-Fos. It is possible that above two responses in concern enhanced the LFP response at a preferential frequency of 3–10 Hz. Long-range as well as local recurrent circuits also appear to be involved since the LFP response does not always coincide with the light illumination [40,41]. The spread of activity was evidenced by the fact that there were many c-Fos neurons that were negative for ChRGR in a region of the motor cortex. Some of them are suggested to project to spinal cord motor neurons directly or indirectly [42,43] as the light-evoked cortical responses were accompanied by enhanced EMG responses.

The LFP power was indeed small at any frequency band under anesthesia. Therefore, the local network appears to be in a stable basin state where the afferent inputs, if any, hardly shift it to the activated semistable state [44]. Our opto-current-clamp study suggests that the depolarization of a small number of neurons wakes up the motor cortical network over some critical point to the activated state where the positive feedback implemented by the recurrent connections maintains a high probability of firing and generates the efferent output to the spinal cord [45].

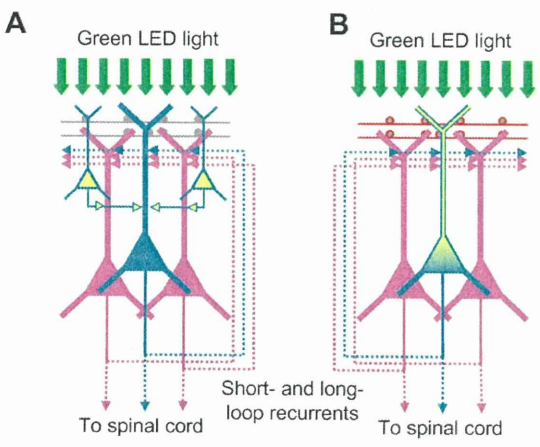

Figure 7. Two hypotheses on the opto-current-clamp actuation of the cortical circuits. A. The green LED light may directly fire the neurons in the surface layers (yellow), but not those in the deep layers (dark green). **B.** The green LED light may directly drive the ChRGR-expressing L5 pyramidal neuron with the intrinsic synaptic bombardments (red boutons) on the tufted apical dendrites.
doi:10.1371/journal.pone.0012893.g007

Materials and Methods

Ethics Statement

All animal experiments were approved by the Tohoku University Committee for Animal Experiments (Approval No. 21LsA-44) and were carried out in accordance with the Guidelines for Animal Experiment and Related Activities in Tohoku University as well as the guiding principles of the Physiological Society of Japan and the NIH.

Plasmid Construction and Expression

Chimeric channelopsins (chops) between chop1 (amino acids 1–345; accession number, AB058890/AF385748, a generous gift from Dr. T. Takahashi, Toho University, Japan) and chop2(1–315) (accession number, AB058891/AF461397, a generous gift from Dr. G. Nagel, Universität Würzburg, Germany) with 5′-EcoRI and 3′-BamHI restriction sites were constructed by overlap extension PCR as described previously [23] using KOD plus DNA polymerase (Toyobo, Osaka, Japan). A chimeric chop fragment was obtained, purified, digested by EcoRI and BamHI and subcloned in-frame into the plasmid pVenus-N1 which has the Venus construct (a generous gift from Dr. A. Miyawaki, RIKEN BSI, Japan) [22]. Coding regions in all constructed plasmids were fully sequenced to verify that no undesired mutations had been introduced by PCR. HEK293 cells were cultured at 37°C and 5% CO_2 in D-MEM (Wako, Osaka, Japan) supplemented with 10% fetal bovine serum and transfected using Effectene Transfection Reagent (Qiagen, Tokyo, Japan) according to the manufacturer's instructions. Twenty-four hours post transfection, the cells were replated onto the collagen-coated glass coverslips for the electrophysiology. We did not supplement the culture and experimental media with retinal, but observed enough large photocurrents for the following experiments.

Evaluation of photocurrents

HEK cells were prepared for electrophysiological recordings 48 hours after transfection. Fluorescence-labeled isolated cells were identified under conventional epi-fluorescence microscopy (BH2-RFC, Olympus, Tokyo, Japan) equipped with a 60× water-immersion objective (LUMplanPl/IR60x, Olympus). The photocurrents were recorded under the whole-cell patch clamp of a conventional system consisting of an amplifier (EPC 8, HEKA Elektronik Dr. Schulze GmbH, Germany) and A/D converter (Digidata 1200B, Molecular Devices Co., Sunnyvale, CA) The standard patch pipette solution contained (in mM), 120 CsOH, 100 glutamate, 50 HEPES, 2.5 MgCl, 2.5 MgATP, 5 Na_2EGTA, 1.2 leupeptin (Sigma) and pH 7.2, adjusted by 1N CsOH. The

access resistance was 10–20 MΩ and was monitored throughout the recording. The cells were continuously superfused (1–2 ml/min) by standard Tyrode solution (in mM:138 NaCl, 3 KCl, 1 $CaCl_2$, 1 $MgCl_2$, 10 HEPES, 4 NaOH, 11 glucose, pH 7.4 by 1N HCl). Most of the experiments were performed at room temperature (27–30°C) unless otherwise noted. For studying the I–V relationship, Cs in the patch pipette solution was replaced with Na, and the liquid junctional potentials of −8 mV were corrected for. For the wavelength-response relationship monochromatic light at 400–560 nm (width, 10 nm) of 1 s duration was applied every 20 s under a conventional epifluorescence system equipped with a Xenon lamp and electromagnetic shutter (CAM-230, JASCO, Tokyo, Japan). Usually the photocurrent was measured by 2–3 repeats of a protocol, in which the wavelength was changed in the order of 460, 480, 500, 520, 540, 560, 560, 540, 520, 500, 480, 460, 440, 420, 400, 400, 420, 440 and 460, and was averaged for each wavelength. The light power density at each wavelength was directly measured by a thermopile (MIR-100Q, Mitsubishi Oil Chemicals, Tokyo, Japan), and was (in $mWmm^{-2}$) 0.021 (400 nm), 0.018 (420 nm), 0.027 (440 nm), 0.027 (460 nm), 0.018 (480 nm), 0.021 (500 nm), 0.015 (520 nm), 0.014 (540 nm) or 0.012 (560 nm), respectively. To investigate the action spectrum, the amplitude of the peak photocurrent at each wavelength was divided by the light power density, multiplied by the wavelength and normalized to the value at 480 nm. For analysis of the photocurrent (I)-voltage (V) relationship and the photocurrent kinetics we used a green LED (505±15 nm, LXHL-NE98, Lumileds Lighting Inc. San Jose, CA) regulated by a pulse generator (SEN-7203, Nihon Kohden, Tokyo, Japan) and computer software (pCLAMP 9, Molecular Devices Co.). The maximal light power density of LED light was 0.77 $mWmm^{-2}$ at the focus. The effective conductance was calculated for each cell by dividing the slope of the I–V relationship between −48 and 32 mV by the input capacitance. The effective conductance was compared as relative to that of ChR1. The turning-on (ON) and -off (OFF) transitions were analyzed by fitting the photocurrent using the simplex method of non-linear least-squares protocol of the appropriate software (Clampfit 9.2 and 10.1 Molecular Devices Co.).

Sindbis pseudovirions transfection

A fragment of ChRGR-Venus was generated by PCR and subcloned into pSinRep5 (Invitrogen). The recombinant Sindbis pseudovirion was generated according to the manufacturer's instructions. Briefly, RNAs were transcribed from this plasmid and DH(26S) helper DNA using MEGAscript SP6 Kit (Ambion, Austin, TX). BHK cells were electroporated with these RNAs and were grown for 24 hr at 37°C, 5% CO_2 in α-MEM containing 5% fetal bovine serum before collecting the supernatant. The titer tested on BHK cells, determined after counting the fluorescent cells infected with serial dilution of the virus stocks, was 1.9×10^6 infectious particles per ml. Recombinant viral stocks were stored at −80°C.

All experiments were done using male C57BL/6J mice (2–3 weeks-old, 7–10 gBW) under anaesthetized by intraperitoneal injection of ketamine-xylazine mixture (50 mg/kgBW ketamine, Daiichi Sankyo Co. Ltd., Tokyo, Japan and 10 mg/kgBW xylazine, Sigma-Aldrich, St. Louis, MO, USA). The viral solution was stereotaxically injected into the primary motor area of the right hemisphere with the following coordinates: anteroposterior from bregma 0.33 mm, lateral from bregma 1.58 mm and ventral 0.5 mm. The body temperature was kept at 37°C by a chemical bedding heater during whole surgery.

Electrophysiology of L5 pyramidal neurons

Twelve hours after injection of the Sindbis pseudovirion vectors, the mice were ether-anesthetized, killed and the cerebral cortex was quickly removed. Sagittal brain slices 250 μm in thickness were prepared using a vibratome (Leica, VT1000s, Wetzlar, Germany) in ice-cold cutting buffer (in mM: 229 Mannitol, 3 KCl, 26 $NaHCO_3$, 1 H_3PO_4, 7 $MgCl_2$ and 11 glucose) bubbled with mixed gas containing 95% O_2 and 5% CO_2. Brain slices were further incubated in artificial cerebrospinal fluid (in mM: 114 NaCl, 2.5 KCl, 26 $NaHCO_3$, 1 NaH_2PO_4, 10 Mannitol, 1.25 $MgCl_2$, 2.5 $CaCl_2$ and 11 glucose) bubbled with the above described mixed gas at 34°C for one hour for the recovery. Although high levels of acetylcholine have been suggested to set the L5 pyramidal neurons to the appropriate dynamics in an awake animal [46,47], the cholinergic tone was absent in the slice. Therefore, it was artificially restored by bath application of the nonhydrolyzable cholinergic agonist carbachol (5 μM, Nacalai Tesque, Kyoto, Japan).

The ChRGR-Venus-expressing layer 5 (L5) pyramidal neurons were visually identified in an acute slice of cerebral cortex under conventional epi-fluorescent microscopy system (BH-2, Olympus Optical Co., Tokyo, Japan) equipped with a 60× water-immersion objective (LUMplanPl/IR60x, Olympus) and a conventional filter cube (excitation, 495 nm; dichroic mirror, 505 nm; barrier filter, 515 nm). Electrophysiological recording was performed at 34±2°C (UTC-1000, Ampere Inc., Tokyo, Japan) under the whole-cell patch clamp from the soma using an amplifier (EPC 8, HEKA Elektronik Dr. Schulze GmbH, Germany). The patch pipette solution was composed of (in mM) 115 potassium gluconate, 20 KCl, 10 HEPES, 2 $MgCl_2$, 0.2 Na_2EGTA, 2.5 MgATP, 0.3 Na_2GTP and 1.2 leupeptin (Sigma-Aldrich) (pH 7.2 by 1 N KOH). In some experiments, biocytin (2 mg/mL, Sigma-Aldrich) was included for the following morphological studies. The pipette resistance, measured directly, was 3.09±0.30 MΩ (n = 16). The liquid junction potential, directly measured, was −9.0 mV and was compensated for. To illuminate the light on the L5 pyramidal neuron under the patch clamp we used the same green LED system as for HEK293 cells. The oscillatory LED light was generated according to the following voltage change [48]:

$$V(t) = V_{\min} + V_{\max}\sin[2\pi f(t)t], \tag{1}$$

where $V_{\min}$ and $V_{\max}$ are the minimal and the maximal voltages driving the LED. The oscillation frequency is swept from the minimal frequency, $f_{\min}$, to the maximal frequency, $f_{\max}$, following the equation [27]:

$$f(t) = f_{\min}\left(e^{Lt} - 1\right)/L, \tag{2}$$

where

$$L = \log(f_{\max}/f_{\min}). \tag{3}$$

However, since the LED light power density was 0 during $V < V_{\min}$, only a positive range of the above function was employed (the rectified sinusoidal sweep of light, RSSL).

Data were low-pass filtered at 1 kHz, sampled digitally at 2 kHz using an A/D converter (Digidata 1200B, Molecular Devices Co.) with a software (Clampex 9.2, Molecular Devices Co.) and analyzed by other software (Clampfit 10.2, Molecular Devices Co.).

Local field potentials (LFP) and electromyogram (EMG)

All the experiments were performed 12 hours after viral injection. At first, mice were anesthetized by intraperitoneal

injection of ketamine-xylazine mixture (50 mg/kgBW ketamine, Daiichi Sankyo Co. Ltd. and 10 mg/kgBW xylazine, Sigma-Aldrich). The anesthesia was maintained during the recording by adding small amounts of ketamine-xylazine mixture every 30 min. The head of each mouse was fixed on the stage of the microscope (Labophoto, Nikon, Tokyo, Japan) using tooth and ear bars. A small area (diameter, 2 mm) was craniotomized using a dental drill while the dura was kept intact. A recording electrode was made from coated stainless steel wire (0.1 mm), inserted stereotaxically into the injected site at the right hemisphere, while the reference electrode was inserted into the left hemisphere according to stereotaxial coordinates (anteroposterior −0.42 mm from bregma; lateral −1.58 mm from bregma). Both LFP electrodes were fixed on the skull using dental cement (Fuji I, GC Co., Tokyo, Japan). To record the EMG, two coated stainless steel wires with straight bared ends (0.1 mm) were directly inserted into extensor muscles of the left forelimb, triceps brachii and carpi radialis brevis, respectively. Another wire was inserted into the triceps brachii muscle of the right forelimb as control. A green LED (505±15 nm, LXHL-NE98, Lumileds Lighting Inc.) was driven by a custom-made booster and computer software (pCLAMP 9, Molecular Devices Co.) and focused on the dura membrane through a microscope objective (WPlan 10, Olympus). The maximal LED light power density was 1.12 $mWmm^{-2}$ on the focal plane. Both LFP and EMG signals were band-pass-filtered (1–300 Hz) by a custom-made amplifier (×100,000) sampled at 1 kHz and stored in the computer by software (Clampex 9, Molecular Devices Co.). The power spectra of LFP or EMG were extracted from 10 repetitive traces using Clampfit 10.2 software and averaged for the statistical analysis.

We analyzed the time-frequency energy distribution of the stimulation-evoked response by continuous wavelet transformation [49]. We used the following equation:

$$Gw(b,a) = \int \frac{1}{\sqrt{a}} \overline{\psi(\frac{t-b}{a})} x(t)dt \quad (4)$$

$$\psi(t) = \frac{1}{2\sqrt{\pi\sigma}} e^{-t^2/\sigma^2} e^{-jt} \quad (5)$$

where x(t) is the evoked response in time (t) domain, $\Psi(t)$ is the mother wavelet, a and b are the scaling factor and translation, respectively. For the mother wavelet, we used the Gabor function in equation (2) with σ being the central frequency of 2 Hz. We varied the scaling factor a to explore frequencies ranging from 1 to 100 Hz. The above equation (1) yielded a series of coefficients that represent the temporal evolution of the frequency content, which were plotted on a pseudocolored 2D graph.

Immunohistochemistry

To investigate the morphological features of the recorded neurons, the cortical slices were immediately fixed after a series of experiments with 4% paraformaldehyde (PFA) in PBS (0.1 M, pH 7.4) for 30 min at 4°C and then washed in PBS. After replacing with 30% sucrose (w/v), each of them was further sliced into 20 µm-thick sections using a freezing microtome (CM 3050S, Leica). The slices were blocked in PBS including 5% normal donkey serum, 0.1% Triton X-100 and 0.25% λ-carrageenan overnight, then treated with the following primary antibodies in PBS including 5% donkey serum and 0.1% Triton X-100. They were reacted with rabbit anti-EGFP IgG (1:1,000; a generous gift from Drs T. Kaneko and K. Nakamura, Kyoto University, Japan) at 4°C for 24 hours and then with anti rabbit IgG (Alexa Fluor 488 conjugate, 1:500, Molecular Probes, Oregon, USA) and streptavidin (Alexa Fluor 546 conjugate, 1:500, Molecular Probes, Oregon USA) at room temperature for 5–6 hours. Finally the slices were mounted with Permafluor (Immunotech, Marseille, France) and coverslipped.

To investigate the c-Fos expression, the anesthetized mice were transcardially perfused with 0.01M PBS, then with 4% paraformaldehyde (PFA) in PBS immediately after the above electrophysiological recordings. The pre-fixed brains were removed, and post-fixed overnight in 4% PFA at 4°C. For cryoprotection, the brains were kept overnight in a PBS solution each with graded concentrations of sucrose from 10 to 30% (w/v). The slices were cut into 16-µm-thick coronal sections on a freezing microtome (CM 3050S, Leica). The sections were washed in 0.025 M PBS followed by blocking buffer (2.5% normal goat serum, 0.1% Triton X-100 and 0.25% λ-carrageenan in PBS), incubated with anti-c-Fos rabbit antibody (Ab-5, 1:1,000, Calbiochem-Merk KGaA, Darmstadt, Germany) and anti-GFP rat antibody (1:500, Nacalai Tesque Inc. Kyoto, Japan) for 48 hours at 4°C. Then, the sections were incubated for 3 hours with biotinylated anti-rabbit-IgG goat antibody (1:200, Jackson, PA, USA). Finally, the slices were treated with streptavidin (Alexa Fluor 546 conjugate, 1:200, Molecular Probes) and anti-rat IgG (Alexa Fluor 488 conjugate, 1:200, Molecular Probes) for fluorescence visualization. The incubation was carried out at room temperature in the blocking buffer, followed by a rinse with PBS. Thereafter, the slices were mounted with Permafluor (Immunotech) and coverslipped.

Each specimen was analyzed three-dimensionally with a z-axis interval of 0.60–0.64 µm under conventional confocal laser-microscopy (LSM510META, Carl Zeiss, Oberkochen, Germany) equipped with a 40× objective unless otherwise noted. The images were corrected for brightness and contrast using conventional software (LSM Image Browser and ImageJ, http://rsb.info.nih.gov/ij/).

Statistics

All data in the text and figures are presented as means ± S.E.M. (number of observations). Statistical significance was tested by the Wilcoxon signed-ranks test for paired data and by the Mann–Whitney U-test for unpaired data. The significance limit was set at $P = 0.05$ in all tests.

Supporting Information

Table S1 Basic electrophysiological parameters of L5 pyramidal neurons.
Found at: doi:10.1371/journal.pone.0012893.s001 (0.04 MB PDF)

Figure S1 Photocurrent amplitude of ChRGR. ChRGR (ChR1-*fg2*) was expressed in a HEK cell and its photocurrent was measured at each wavelength. Here, the ChRGR photocurrent (green diamond) was compared with the corresponding photocurrent of either ChR2 (blue circle), ChR2-H134R (light blue triangle), or VChR1 (yellow square). A, C, E. the peak currents (I_{peak}). B, D, F. the steady-state photocurrents (I_{ss}). Each symbol and bars are mean and SEM of data, n = 8 (ChRGR), n = 8 (ChR2), n = 9 (ChR2-H134R) and n = 6 (VChR1). * indicates that the difference was significant ($P<0.05$, Mann-Whitney U-test). The light power density at each wavelength was (in $mWmm^{-2}$) 0.021 (400 nm), 0.018 (420 nm), 0.027 (440 nm), 0.027 (460 nm), 0.018 (480 nm), 0.021 (500 nm), 0.015 (520 nm), 0.014 (540 nm) or 0.012 (560 nm), respectively. It was relatively small at 480 nm

and over 520 nm because of the spectral properties of the light source (Xenon arc lamp).
Found at: doi:10.1371/journal.pone.0012893.s002 (0.06 MB PDF)

Figure S2 Membrane properties of ChRGR-Venus-expressing neurons. A. Membrane potential responses (bottom traces) to current injections from the patch electrode (top). B. Frequency of action potentials as a function of injected current; ChRGR-Venus-expressing neurons and non-expressing controls. C. Typical current-clamp responses of a L5 pyramidal neuron to the green LED pulses. The external solution included 1 μM TTX to suppress the generation of action potentials. The resting potential was −73 mV and the membrane time constant was 104 ms.
Found at: doi:10.1371/journal.pone.0012893.s003 (0.06 MB PDF)

Figure S3 Frequency responsiveness of neuronal membrane potential. The rectified sinusoidal sweep of light (RSSL) from 0.1 to 100 Hz (top green), the photocurrent response of an L5 pyramidal neuron under voltage clamp (*I*, brown), and the membrane potential (*V*, blue) from the same neuron. To suppress the generation of action potentials, TTX (1 μM) was included in the external solution. Note that the membrane potential change became small with the increase of frequency because of the large membrane time constant of this neuron (33 ms).
Found at: doi:10.1371/journal.pone.0012893.s004 (0.05 MB PDF)

Figure S4 Non-linear photocurrent responses. The peak (magenta diamond) and steady-state photocurrent amplitude (closed circle) as functions of green LED power density. The lines were drawn fitting to Michaelis-Menten relationship: peak (K_D, 0.10 $mWmm^{-2}$; I_{max}, 0.19 nA) and steady-state (K_D, 0.10 $mWmm^{-2}$; I_{max}, 0.17 nA). Recorded from ChRGR-expressing L5 pyramidal neurons (mean ± SEM, n = 4).
Found at: doi:10.1371/journal.pone.0012893.s005 (0.04 MB PDF)

Figure S5 Distribution of ChRGR-expressing neurons. (Left) The number of neurons expressing ChRGR-Venus was estimated for each depth. The ChRGR-expressing neurons which also expressed c-Fos at higher levels were counted as indicated in white columns. (Right) The LFP (black lines) and EMG (red lines) recorded from each animal. The data from mouse #2 was typical and used in the text-figure 3. Methods: The post-fixed mouse brain was sliced into 16-mm-thick coronal sections on a freezing microtome (CM 3050S, Leica) and immunohistochemically labeled with anti-EGFP and anti-c-Fos. The numbers of fluorescent neurons were counted under confocal microscopy (LSM510META, Oberkochen, Germany) using one of every 5 slices (80 μm). Total numbers of neurons were estimated for each depth window by linear estimation. As for anti-c-Fos, the intensity of fluorescence was variable from one cell to another. The cell expressing c-Fos at a higher level was visually identified relative to the background fluorescence.
Found at: doi:10.1371/journal.pone.0012893.s006 (0.32 MB PDF)

Figure S6 Photocurrent kinetics of ChR2-H134R. A–C. ChR2-H134R was expressed in a HEK cell and its photocurrent was evoked by 1s pulse of green LED of various strenth (light blue triangle, mean and SEM). (A) The apparent ON time constant (τ_{ON})-light power density relationships. (B) The effective OFF time constant (τ_{OFF})-light power density relationships. (C) The desensitization-light power density relationships. D. The recovery time course of the desensitizing component. The process was fitted to a single exponential relationship (time constant, 3 s). Each green line is the relationship obtained from ChRGR that is copied from text-Figure 2D–F or 2J.
Found at: doi:10.1371/journal.pone.0012893.s007 (0.05 MB PDF)

Figure S7 Sensitivity to pH. A and B. ChRGR (ChR1-*fg2*) was expressed in a HEK cell and its photocurrent was measured at each membrane potential of −48 (blue), −28 (magenta), −8 (brown), 12 (green) or 32 mV (purple). The pH of external solution was adjusted to 7.4 (A) or 6.0 (B). C and D. The peak currents (I_{peak}, open diamond) and the steady-state photocurrents (I_{ss}, closed circle) as functions of membrane potential (*V*). pH 7.4 (C) and 6.0 (D). E. The pH sensitivity of τ_{OFF}. The difference was significant ($P<0.01$, Mann-Whitney *U*-test). F. The pH sensitivity of τ_{ON}. G. The pH sensitivity of desensitization.
Found at: doi:10.1371/journal.pone.0012893.s008 (0.05 MB PDF)

Acknowledgments

We thank G. Nagel and T. Takahashi for the channelrhodopsin cDNA, K. Deisseroth for the *Volvox* channelrhodopsin plasmid, M. Prigge and P. Hegemann for the ChR2-H134R plasmid, A. Miyawaki for the *Venus* cDNA, S. Sakai for experimental assistance and discussion, M. Osanai and H. Ohta for comments on the manuscript and B. Bell for the language assistance.

Author Contributions

Conceived and designed the experiments: TI HY. Performed the experiments: LW HW ST RE. Analyzed the data: LW HW. Contributed reagents/materials/analysis tools: YM HM. Wrote the paper: TI HY. Electrophysiological experiments using the cortical slices and the in vivo animal, data analysis, immunohistochemistry, image analysis: LW. Molecular biology of channelrhodopsins, electrophysiological experiments using the expression system, data analysis: HW. Electrophysiological experiments using the expression system: ST RE. Wavelet analysis: YM. Organization of the research group involved in the wavelet analysis: HM. Planning, organization and fund management of research group involved in the molecular biology: TI. Planning, organization and fund management of all research groups: HY. Preparation of the paper: LW HW TI HY.

References

1. Callaway EM, Yuste R (2002) Stimulating neurons with light. Curr Opin Neurobiol 12: 587–592.
2. Miesenböck G (2004) Genetic methods for illuminating the function of neural circuits. Curr Opin Neurobiol 14: 395–402.
3. Callaway EM (2005) A molecular and genetic arsenal for systems neuroscience. Trends Neurosci 28: 196–201.
4. Kramer RH, Fortin DL, Trauner D (2009) New photochemical tools for controlling neuronal activity. Curr Opin Neurobiol 19: 544–552.
5. Miesenböck G (2009) The optogenetic catechism. Science 326: 395–399.
6. Sineshchekov OA, Jung KH, Spudich JL (2002) Two rhodopsins mediate phototaxis to low- and high-intensity light in *Chlamydomonas reinhardtii*. Proc Natl Acad Sci U S A 99: 8689–8694.
7. Suzuki T, Yamasaki K, Fujita S, Oda K, Iseki M, et al. (2003) Archaeal-type rhodopsins in Chlamydomonas: model structure and intracellular localization. Biochem Biophys Res Commun 301: 711–717.
8. Nagel G, Ollig D, Fuhrmann M, Kateriya S, Musti AM, et al. (2002) Channelrhodopsin-1: a light-gated proton channel in green algae. Science 296: 2395–2398.
9. Nagel G, Szellas T, Huhn W, Kateriya S, Adeishvili N, et al. (2003) Channelrhodopsin-2, a directly light-gated cation-selective membrane channel. Proc Natl Acad Sci U S A 100: 13940–13945.
10. Li X, Gutierrez DV, Hanson MG, Han J, Mark MD, et al. (2005) Fast noninvasive activation and inhibition of neural and network activity by vertebrate rhodopsin and green algae channelrhodopsin. Proc Natl Acad Sci U S A 102: 17816–17821.

11. Huber D, Petreanu L, Ghitani N, Ranade S, Hromádka T, et al. (2008) Sparse optical microstimulation in barrel cortex drives learned behaviour in free moving mice. Nature 451: 61–64 (2007).
12. Zhang YP, Oertner TG (2007) Optical induction of synaptic plasticity using a light-sensitive channel. Nat Methods 4: 139–141.
13. Han X, Qian X, Bernstein JG, Zhou HH, Franzesi GT, et al. (2009) Millisecond-timescale optical control of neural dynamics in the nonhuman primate brain. Neuron 62: 191–198.
14. Nagel G, Brauner M, Liewald JF, Adeishvili N, Bamberg E, et al. (2005) Light activation of channelrhodopsin-2 in excitable cells of *Caenorhabditis elegans* triggers rapid behavioral responses. Curr Biol 15: 2279–2284 (2005).
15. Douglass AD, Kraves S, Deisseroth K, Schier AF, Engert F (2008) Escape behavior elicited by single, channelrhodopsin-2-evoked spikes in zebrafish somatosensory neurons. Curr Biol 18: 1133–1137.
16. Arenkiel BR, Peca J, Davison IG, Feliciano C, Deisseroth K, et al. (2007) In vivo light-induced activation of neural circuitry in transgenic mice expressing channelrhodopsin-2. Neuron 54: 205–218.
17. Tomita H, Sugano E, Fukazawa Y, Isago H, Sugiyama Y, et al. (2009) Visual properties of transgenic rats harboring the channelrhodopsin-2 gene regulated by the thy-1.2 promoter. PLoS One 4: e7679.
18. Bi A, Cui J, Ma YP, Olshevskaya E, Pu M, et al. (2006) Ectopic expression of a microbial-type rhodopsin restores visual responses in mice with photoreceptor degeneration. Neuron 50: 23–33.
19. Lagali PS, Balya D, Awatramani GB, Münch TA, Kim DS, et al. (2008) Light-activated channels targeted to ON bipolar cells restore visual function in retinal degeneration. Nat Neurosci 11: 667–675.
20. Tomita H, Sugano E, Yawo H, Ishizuka T, Isago H, et al. (2007) Restoration of visual response in aged dystrophic RCS rats using AAV-mediated channelopsin-2 gene transfer. Invest Ophthalmol Vis Sci 48: 3821–3826.
21. Hegemann P, Ehlenbeck S, Gradmann D (2005) Multiple photocycles of channelrhodopsin. Biophys J 89: 3911–3918.
22. Ishizuka T, Kakuda M, Araki R, Yawo H (2006) Kinetic evaluation of photosensitivity in genetically engineered neurons expressing green algae light-gated channels. Neurosci Res 54: 85–94.
23. Wang H, Sugiyama Y, Hikima T, Sugano E, Tomita H, et al. (2009) Molecular determinants differentiating photocurrent properties of two channelrhodopsins from chlamydomonas. J Biol Chem 284: 5685–5696.
24. Nagel G, Szellas T, Kateriya S, Adeishvili N, Hegemann P, et al. (2005) Channelrhodopsins: directly light-gated cation channels. Biochem Soc Trans 33: 863–866 (2005).
25. Zhang F, Prigge M, Beyrière F, Tsunoda SP, Mattis J, et al. (2008) Red-shifted optogenetic excitation: a tool for fast neural control derived from *Volvox carteri*. Nat Neurosci 11: 631–633.
26. Gutfreund Y, Yarom Y, Segev I (1995) Subthreshold oscillations and resonant frequency in guinea-pig cortical neurons: physiology and modeling. J Physiol 483: 621–640.
27. Tohidi V, Nadim F (2009) Membrane resonance in bursting pacemaker neurons of an oscillatory network is correlated with network frequency. J Neurosci 29: 6427–6435.
28. Sugiyama Y, Wang H, Hikima T, Sato M, Kuroda J, et al. (2009) Photocurrent attenuation by a single polar-to-nonpolar point mutation of channelrhodopsin-2. Photochem Photobiol Sci 8: 328–336.
29. Sheng M, Greenberg ME (1990) The regulation and function of c-fos and other immediate early genes in the nervous system. Neuron 4: 477–485.
30. Guzowski JF, Setlow B, Wagner EK, McGaugh JL (2001) Experience-dependent gene expression in the rat hippocampus after spatial learning: a comparison of the immediate-early genes Arc, c-fos, and zif268. J Neurosci 21: 5089–5098.
31. Schoenenberger P, Gerosa D, Oertner TG (2009) Temporal control of immediate early gene induction by light. PLoS One 4: e8185.
32. Gunaydin LA, Yizhar O, Berndt A, Sohal VS, Deisseroth K, et al. (2010) Ultrafast optogenetic control. Nat Neurosci 13: 387–392.
33. Boyden ES, Zhang F, Bamberg E, Nagel G, Deisseroth K (2005) Millisecond-timescale, genetically targeted optical control of neural activity. Nat Neurosci 8: 1263–1268.
34. Hutcheon B, Yarom Y (2000) Resonance, oscillation and the intrinsic frequency preferences of neurons. Trends Neurosci 23: 216–222.
35. Cardin JA, Carlén M, Meletis K, Knoblich U, Zhang F, et al. (2009) Driving fast-spiking cells induces gamma rhythm and controls sensory responses. Nature 459: 663–667.
36. Sohal VS, Zhang F, Yizhar O, Deisseroth K (2009) Parvalbumin neurons and gamma rhythms enhance cortical circuit performance. Nature 459: 698–702.
37. Weiler N, Wood L, Yu J, Solla SA, Shepherd GM (2008) Top-down laminar organization of the excitatory network in motor cortex. Nat Neurosci 11: 360–366.
38. Destexhe A, Contreras D (2006) Neuronal computations with stochastic network states. Science 314: 85–90.
39. Larkum ME, Nevian T, Sandler M, Polsky A, Schiller J (2009) Synaptic integration in tuft dendrites of layer 5 pyramidal neurons: a new unifying principle. Science 325: 756–760.
40. Striade M (2000) Corticothalamic resonance, states of vigilance and mentation. Neuroscience 101: 243–276.
41. Douglas RJ, Martin KA (2004) Neuronal circuits of the neocortex. Annu Rev Neurosci 27: 419–451.
42. Kalil K (1984) Development and regrowth of the rodent pyramidal tract. Trends Neurosci 7: 394–398.
43. Terashima T (1995) Anatomy, development and lesion-induced plasticity of rodent corticospinal tract. Neurosci Res 22: 139–161.
44. Rolls ET, Loh M, Deco G (2008) An attractor hypothesis of obsessive-compulsive disorder. Eur J Neurosci 28: 782–793.
45. Haider B, McCormick DA (2009) Rapid neocortical dynamics: cellular and network mechanisms. Neuron 62: 171–189.
46. Hasselmo ME, Giocomo LM (2006) Cholinergic Modulation of Cortical Function. J Mol Neurosci 30: 133–135.
47. van der Zee EA, Luiten PG (1999) Muscarinic acetylcholine receptors in the hippocampus, neocortex and amygdale: a review of immunocytochemical localization in relation to learning and memory. Prog Neurobiol 58: 409–471 (1999).
48. Puil E, Gimbarzevsky B, Miura RM (1986) Quantification of membrane properties of trigeminal root ganglion neurons in guinea pigs. J Neurophysiol 55: 995–1016.
49. Sutoh T, Yabe H, Sato Y, Hiruma T, Kaneko S (2000) Event-related desynchronization during an auditory oddball task. Clin Neurophysiol 111: 858–862.

Development, Growth & Differentiation
The Japanese Society of Developmental Biologists

Develop. Growth Differ. (2011) **53**, 357–365 doi: 10.1111/j.1440-169X.2010.01235.x

Original Article

Differentiation of neuronal cells from NIH/3T3 fibroblasts under defined conditions

Zhuo Wang, Eriko Sugano, Hitomi Isago, Teru Hiroi, Makoto Tamai and Hiroshi Tomita*

Tohoku University Institute for International Advanced Interdisciplinary Research, 4-1 Seiryo-machi, Aoba-ku, Sendai 980-8575, Japan

We attempted to test whether the differentiated NIH/3T3 fibroblasts could be differentiated into neuronal cells without any epigenetic modification. First, a neurosphere assay was carried out, and we successfully generated neurosphere-like cells by floating cultures of NIH/3T3 fibroblasts in neural stem cell medium. These spheres have the ability to form sub-spheres after three passages, and express the neural progenitor markers Nestin, Sox2, Pax6, and Musashi-1. Second, after shifting to a differentiating medium and culturing for an additional 8 days, cells in these spheres expressed the neuronal markers β-tubulin and neurofilament 200 and the astrocytic marker glial fibrillary acidic protein (GFAP). Finally, after treating the spheres with all-trans retinoic acid and taurine, the expression of β-tubulin was increased and the staining of photoreceptor markers rhodopsin and recoverin was observed. The present study shows that NIH/3T3 fibroblasts can generate neurosphere-like, neuron-like, and even photoreceptor-like cells under defined conditions, suggesting that the differentiated non-neuronal cells NIH/3T3 fibroblasts, but not pluripotent cells such as embryonic stem cells or induced pluripotent stem cells, may have the potential to be transdifferentiated into neuronal cells without adding any epigenetic modifier. This transdifferentiation may be due to the possible neural progenitor potential of NIH/3T3 fibroblasts that remains dormant under normal conditions.

Key words: differentiation, neural progenitors, neuron, retinoic acid, taurine.

Introduction

Because of their ability to proliferate infinitely and differentiate into cells of all three germ layers, embryonic stem (ES) cells are regarded as superior potential donor cells for cell replacement to treat many diseases (Hoffman & Carpenter 2005; Takahashi & Yamanaka 2006), such as retinitis pigmentosa and age-related macular degeneration, which are typically characterized by the death of photoreceptors (Osakada *et al.* 2008). Photoreceptor replacement in the form of a cell-based therapeutic approach may aid in the restoration of vision.

Zhao *et al.* (2002) demonstrated that ES cell-derived neural progenitors expressed regulatory factors needed for retinal differentiation, and that a small subset of these cells differentiated along the photoreceptor lineage in response to retina-specific epigenetic cues. Ikeda *et al.* (2005) and Osakada *et al.* (2008) generated putative photoreceptors and RPE cells from rodent and primate ES cells by induction with defined factors.

However, in clinical application, the use of ES cells involves ethical problems and immune rejection. Jin *et al.* (2009) demonstrated partial mesenchymal stem cells obtained from umbilical cord blood were able to be differentiated into neuron-like cells or rhodopsin-positive cells *in vitro*. Recently, retinal cells have been generated from mouse- and human-induced pluripotent stem (iPS) cells by introducing four specific factors Oct3/4, Sox2, Klf4, and c-Myc (Takahashi & Yamanaka 2006; Hirami *et al.* 2009; Osakada *et al.* 2009).

Even though the generation and application of iPS cells made it possible to treat patients with their own cell-derived retinal cells, which may resolve the problem of immune rejection, some questions still remain. For example, the introduction of viral vectors and oncogenes c-Myc and Klf4 into the somatic genome limits the utility of iPS cells for patient-specific therapy

*Author to whom all correspondence should be addressed.
Email: hiroshi-tomita@iiare.tohoku.ac.jp
Received 28 June 2010; revised 30 November 2010; accepted 30 November 2010.

(Yamanaka 2007, 2009; Zhou *et al.* 2009). Furthermore, the generation of an iPS cell line takes considerable time (approximately 6 months) and is labor intensive so it can not be generated rapidly (Holden & Vogel 2008).

In the previous studies, most investigators have used undifferentiated cells, such as ES cells, ES cell-derived neural progenitors, bone marrow stromal cells, or iPS cells, as the cell source (Sanchez-Ramos *et al.* 2000; Woodbury *et al.* 2000; Zhao *et al.* 2002; Ikeda *et al.* 2005; Klassen & Reubinoff 2008; Osakada *et al.* 2008; Jin *et al.* 2009). Zhang *et al.* (2010) showed that NIH/3T3 fibroblasts, which are already committed to a specific differentiation destiny, were able to be induced to express neuronal markers, but these cells have to be reprogrammed by adding epigenetic modifiers to make epigenetic modification.

NIH/3T3 fibroblasts, derived from an embryo of the NIH/Swiss mouse, are generally adherently cultured in Dulbecco's modified Eagle's medium (DMEM) supplemented with 10% bovine calf serum, which is the normal culture condition for most investigators. In the present study, we cultured NIH/3T3 cells in a completely different microenvironment to establish whether this cell line could be induced into neuronal cells without adding any epigenetic modifier and to be further induced into retinal photoreceptor-like cells simply by adding taurine and retinoic acid (RA), and we also characterized the mechanism involved.

Materials and methods

Culture of NIH/3T3 fibroblasts

NIH/3T3 fibroblasts were kindly provided by the Cell Resource Center for Biomedical Research, Tohoku University, Japan as a frozen stock. Cells were adherently cultured in DMEM with 10% newborn calf serum (NCS), 1× GlutaMax, and 1× Antibiotic-Antimycotic (Invitrogen/Gibco) on normal tissue culture dishes (uncoated) at 37°C, 5% CO_2, which is referred to as normal conditions (NC).

Generation of neurosphere-like cells (Neurosphere assay)

Neurosphere assays were carried out according to previous studies (Das *et al.* 2006; Brewer & Torricelli 2007) with minimal modifications. Briefly, NIH/3T3 fibroblasts were cultured in suspension in NC or neural stem cell medium (NSCm) on 2.0% agarose-coated dishes at a density of 1×10^5 cells/mL for 5–7 days to detect the ability of these cells to form spheres. NSCm was serum-free and composed of DMEM/F-12, 1× GlutaMax, 1× Antibiotic-Antimycotic, 1× B27 supplement (without vitamin A: Cat. No. 12587), 1× N2 supplement, 20 ng/mL bFGF (basic fibroblast growth factor), and 20 ng/mL EGF (epidermal growth factor). All reagents were obtained from Invitrogen/Gibco. Adherent NIH/3T3 fibroblasts cultured in NC on normal tissue culture dishes were used as a control.

Passage of neurosphere-like cells

After 5–7 days of cultivation, spheres were trypsinized into single cells and resuspended in NSCm. The suspension was plated onto a new 2.0% agarose-coated dish and cultured for another 5–7 days to test the ability of these cells to form secondary spheres.

To examine the proliferative ability and expression of neural progenitor markers of NIH/3T3-derived spheres, after 7 days of floating cultivation for the second passage, the spheres were exposed to 10 μmol/L BrdU (Sigma) to tag the dividing cells and plated onto poly-D-lysine-coated 8-well culture slides (BD Biosciences) for the final 48 h (Das *et al.* 2006). Immunocytochemistry was carried out for double staining analysis of the neural progenitor markers Nestin, Sox2, Pax6, Musashi-1 (Msi1), and BrdU. RNA was isolated from NIH/3T3 cells cultured in different conditions, and real-time polymerase chain reaction (PCR) were performed to compare the expression of neural progenitor markers Nestin and Sox2.

Differentiation of neuron- and glia-like cells

For the differentiating culture, NSCm-cultured spheres were trypsinized into single cells and resuspended in differentiating medium (DM), then plated onto poly-D-lysine-coated 8-well culture slides and cultured for an additional 8 days. In DM, EGF and B-27 supplement (without RA Cat. No.12587) were replaced by 1% serum and standard B-27 supplement (including retinyl acetate: Cat. No. 17504). In addition, brain-derived neurotrophic factor (BDNF: 10 ng/mL) was added to promote the differentiation into neuronal cells, and ciliary neurotrophic factor (CNTF: 20 ng/mL) was added for glial cell differentiation (Yang *et al.* 2005; Das *et al.* 2006; Chen *et al.* 2007; Chojnacki & Weiss 2008; Matsuda *et al.* 2009). Immunocytochemistry was carried out to stain the markers of neurons (β-tubulin and neurofilament 200 [NF200]), astrocytes (glial fibrillary acidic protein [GFAP]), and oligodendrocytes (O4).

Induction of retinal photoreceptor-like cells

For the induction of retinal photoreceptor-like cells, NIH/3T3-derived neuron-like cells were trypsinized and

resuspended in an induction medium (IM), which is composed of DMEM/F-12 supplemented with 1% NCS, 1× Antibiotic-Antimycotic, 1× Glutamax, 10 ng/mL BDNF and the inducing agent taurine (50 μmol/L) plus RA (10 μmol/L), then plated onto poly-D-lysine-coated 8-well culture slides to culture for an additional 8 days (Das *et al.* 2006; Osakada *et al.* 2008). Cells were fixed and immunocytochemistry was performed by staining the retinal photoreceptor markers rhodopsin and recoverin.

Real-time PCR

Real-time PCR was performed as previously described (Sugano *et al.* 2003). Total RNA was isolated from cultured cells using Trizol (Sigma). cDNA synthesis was carried out using the First-Strand cDNA Synthesis kit (GE Healthcare). SYBR Premix Ex Taq (Perfect Real Time; Takara) was used for PCR reactions. Specific transcripts were amplified on a Smart Cycler (Takara) for 35–40 cycles. The expression level of each gene was calculated by normalizing it with the glyceraldehyde 3-phosphate dehydrogenase (GAPDH) gene (TaqMan Rodent GAPDH Control Reagents; Applied Biosystems). The primers used in the experiment are shown in Table 1.

Immunocytochemical analysis

Immunocytochemistry was performed by staining cell-specific markers as previously described (Sugano *et al.* 2005; Das *et al.* 2006). Briefly, cells were fixed with 4% paraformaldehyde for 10 min at room temperature. After permeabilization with 0.3% Triton X-100 in phosphate-buffered saline (PBS) for 10 min, slides were incubated in 1% bovine serum albumin (BSA) and 5% blocking serum for 30 min at room temperature. Primary antibodies were added and incubated overnight at 4°C. The list of antibodies and their dilution are given in Table 2. Slides were washed and incubated with the secondary antibodies conjugated to Alexa Fluor 594 (red) or Alexa Fluor 488 (green) (Invitrogen-Molecular Probes) in the dark for 30 min at room temperature. A negative control was performed by replacing the primary antibody with normal IgG. For staining of nuclei, cells were covered with Vectashield medium including 4′6′-diamidino-2-phenylindole dihydrochloride (DAPI) (Vector Laboratories Inc.). Fluorescence was excited and labeled cells were imaged with a fluorescence microscope (Axiovert40; Zeiss, Germany).

Protein extraction and western blotting

Western blotting analysis was performed as previously described (Takahashi & Yamanaka 2006). Briefly, the NIH/3T3 cells were lysed with RIPA buffer supplemented with cocktail (Roche), and cell lysates (50 μg) were separated by electrophoresis on Mini-PROTEAN TGX gel (BIO-RAD) and transferred to an immuno-blot PVDF membrane (BIO-RAD). Antibodies used were Sox2, Nestin (1:200, shown in Table 2), anti-rabbit and anti-mouse IgG (H&L) AP conjugate (1: 7500, Promega).

Statistical analysis

The data of real-time PCR analysis are expressed as mean ± SD. Significance between groups was analyzed by one-way analysis of variance (ANOVA) with GraphPad Prism 4.0 software (San Diego). Values of $P < 0.05$ were considered statistically significant.

Results

NIH/3T3 fibroblasts can form neurosphere-like cells in defined conditions

First, we carried out a neurosphere assay on floating NIH/3T3 cells cultured in two different proliferating media: NSCm and NC. When NIH/3T3 cells were cultured in suspension for 2–5 days, NIH/3T3 cells formed spheres (Fig. 1B,C), which displayed classic features of neurospheres, in both proliferating media. There was no apparent difference in morphology between NC- and NSCm-cultured spheres for the first 2–3 days of culture. All NSCm-cultured spheres had a regular and round shape with bright borders on the edge of spheres (Fig. 1B). However, after 4–5 days of culture, the diameter of NC-cultured spheres did not increase, and some of these spheres showed an irregular and unhealthy appearance with dark or indistinct borders (Fig. 1C), which was assumed to be

Table 1. Sequences of primers used in real-time polymerase chain reaction (PCR)

Gene	Primer sequence (5′-3′) F	R	Product (bp)	Annealing temp. (°C)	GeneBank accession number
Nestin	AGACAGTGAGGCAGATGAGT	ATGAGAGGTCAGAGTCATGG	224	55	NM_016701
Sox2†	TAGAGCTAGACTCCGGGCGATGA	TTGCCTTAAACAAGACCACGAAA	296	60	NM_011443

†Primers of Sox2 were from Takahashi & Yamanaka (2006).

Table 2. List of antibodies used to stain different target cells

Antibody	Species	Dilution	Company and catalog no.	Target cells
Nestin	Mouse	1:500	Millipore-Chemicon:MAB353	Neural progenitors
Sox2	Rabbit	1:100	Santa Cruz Biotechnology, Inc: sc-20088	Neural progenitors
Msi1	Rabbit	1:100	Sigma-Aldrich: M3571	Neural progenitors
Pax6	Rabbit	1:100	Santa Cruz Biotechnology, Inc: sc-32766	Neural progenitors
BrdU	Mouse	1:100	Santa Cruz Biotechnology, Inc: sc-32323	Proliferating cells
β-tubulin	Mouse	1:500	Sigma: T5076	Neurons
NF200	Mouse	1:100	Sigma: N0142	Neurons
GFAP	Goat	1:100	Santa Cruz Biotechnology, Inc: sc-6171	Astrocytes
O4	Mouse	1:100	Chemicon International, Inc.: MAB345	Oligodendrocytes
Rhodopsin	Mouse	1:100	Millipore-Chemicon: MAB5316	Photoreceptors
Recoverin	Goat	1:100	Santa Cruz Biotechnology, Inc: sc-20353	Photoreceptors

BrdU, 5-Bromo-2′-deoxyuridine; GFAP, glial fibrillary acicic protein; Msi1, Musashi homologue 1; NF200, neurofilament 200 kDa; O4, oligodendrocyte marker O4; Pax6, paired box protein 6; Sox2, SRY (sex determining region Y)-box containing gene 2.

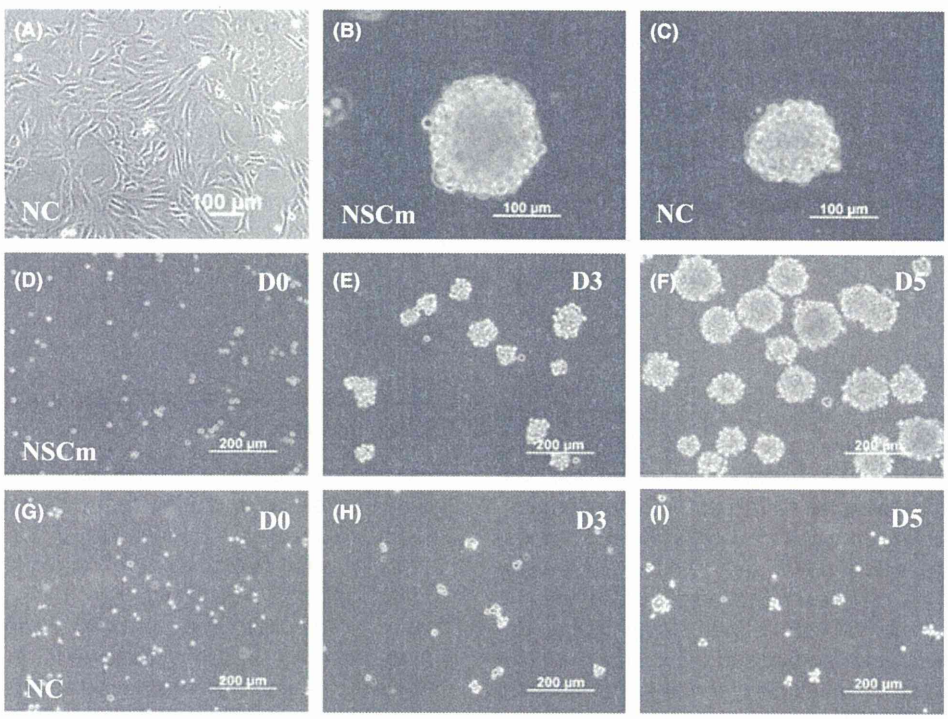

Fig. 1. Generation and passage of NIH/3T3-derived neurosphere-like cells. NIH/3T3 fibroblasts were adherently cultured in normal condition (NC) on normal (uncoated) dishes (A). Spheres were generated after culturing in neural stem cell medium (NSCm) (B) or NC (C) on 2% agarose-coated dishes for 5 days. Generation of the secondary spheres were carried out by culturing in NSCm (D–F) or NC (G–I) for 0, 3, and 5 days. The NSCm-cultured secondary spheres were observed on day 3 (E) after passaging, and the diameter had doubled by day 5 (F). NC-cultured spheres formed very small secondary spheres, and the diameter was unchanged after 3–5 days of culture (H and I).

surrounded by many dying cells caused by the lack of necessary growth factors.

Second, we tested the ability of NIH/3T3-derived spheres to generate secondary spheres. After dissociating into single cells and culturing for 3–7 days, the secondary spheres were quickly formed (on days 3–5) in NSCm, and the sphere size was dependent on culture time with defined cell density (Fig. 1D–F). These cells could generate sub-spheres for an extended period of three passages (more passages were untested). However, NC-cultured spheres formed only very small secondary spheres on days 3–5 after passaging (Fig. 1G–I), and tertiary spheres were difficult to generate.

NIH/3T3-derived spheres express neural progenitor markers

Third, we performed immunocytochemistry to stain the neural progenitor markers Nestin, Sox2, Pax6, and Msi1 for NSCm-cultured NIH/3T3-derived spheres, and the results showed that these cells expressed neural progenitor markers (Fig. 2E–T). Some of these spheres co-expressed Nestin and Sox2 (Fig. 2J–L), suggesting that some cells expressed multiple neural progenitor markers. Double staining for Sox2, Pax6, and Msi1 with BrdU indicated that these spheres were composed of dividing cells that entered the cell cycle (Fig. 2N–P,R,T).

To compare the neural progenitor potential of NIH/3T3 cells cultured in different conditions, the expression of neural progenitor markers Sox2 and Nestin were examined by real-time PCR. Sox2 (Fig. 2V) and Nestin (Fig. 2W) were significantly upregulated in NSCm-cultured spheres compared with adherent NIH/3T3 fibroblasts or NC-cultured spheres. Moreover, the expression of Nestin and Sox2 were also observed from NSCm-cultured spheres by western blotting (Fig. 2X).

NIH/3T3-derived spheres have the potential to differentiate into neuronal cells

Subsequently, we tested whether NIH/3T3-derived spheres can be differentiating into neuronal cells. After transferring to the DM, these spheres were cultured for another 8 days. Immunocytochemical results showed that these cells expressed the neuronal markers β-tubulin (Fig. 3D) and NF200 (Fig. 3H) and the astrocytic marker GFAP (Fig. 3K), although expression of GFAP was very low. However, these cells did not express the oligodendrocyte marker O4 (data not shown).

NIH/3T3-derived spheres can be induced to express retinal photoreceptor markers

Finally, to determine the ability of NIH/3T3 cells to differentiate along neural lineage, we treated NIH/3T3-derived neuron-like cells with taurine and RA, both of which show effective promotion of neuron induction. After treatment with these chemicals, expression of the neuronal marker β-tubulin (Fig. 4E) was greatly enhanced, and expression of photoreceptor markers rhodopsin (Fig. 4I,K,M) and recoverin (Fig. 4L,M) was also induced. Double staining results showed that some cells co-expressed recoverin and rhodospin (Fig. 4K–M); however, the expression of recoverin was very low (Fig. 4L–N). Real-time PCR analysis showed that neural progenitor markers Sox2 and Nestin were significantly downregulated during the differentiation and induction of neuron- and photoreceptor-like cells (Fig. 4O,P).

Discussion

Many studies have shown that the undifferentiated cells, such as ES cells, ES-derived neural stem cells (NSCs), bone marrow stromal cells or iPS cells have the ability to be differentiated along the neuronal lineage (Sanchez-Ramos *et al.* 2000; Woodbury *et al.* 2000; Zhao *et al.* 2002; Ikeda *et al.* 2005; Takahashi & Yamanaka 2006; Osakada *et al.* 2008, 2009; Hirami *et al.* 2009; Jin *et al.* 2009) and could be potential targets for the replacement therapy for retinal degeneration diseases. However, the ability of differentiated cells to be transdifferentiated into neuronal cells has not been widely investigated. Zhang *et al.* (2010) showed that the NIH/3T3 fibroblasts were able to be induced to express neuronal markers after the epigenetic modification by adding epigenetic modifiers, but the question of whether the differentiated cells could be transdifferentiated into neuronal cells without adding any epigenetic modifier and the mechanism involved still remain to be characterized.

Our study showed that NIH/3T3 fibroblasts were able to form spheres composed of dividing cells in suspension culture in the presence of EGF, bFGF and B27 supplement (without vitamin A), which are conditions suitable for the proliferation of neural progenitors. These spheres were able to be serially passaged to form more sub-spheres, and these cells were incorporated with BrdU, indicating their ability to self-renew. NSCm-cultured spheres express neural progenitor markers Nestin, Sox2, Pax6 and Msi1, indicating that these cells may have the potential to proliferate toward neural progenitor lineage. NIH/3T3-derived spheres was able to be differentiated into both neuronal and astrocytic cell types by removing EGF and B27 supplement (without vitamin A) from the medium and substituting them with serum, standard B-27 supplement and BDNF or CNTF, and also have the potential to be induced into photoreceptor-like cells. Taken together, these results suggested that NIH/3T3-derived neurosphere-like cells can undergo self-renewal and differentiation into neuron-like cells without any epigenetic modification, which are properties of neural progenitors, suggesting the possible neuronal lineage of NIH/3T3 fibroblasts.

To test whether the NIH/3T3-derived spheres obtained were neurospheres or neural progenitors, three functional attributes that define neural progenitors (or neural stem cells) must be exhibited. The first

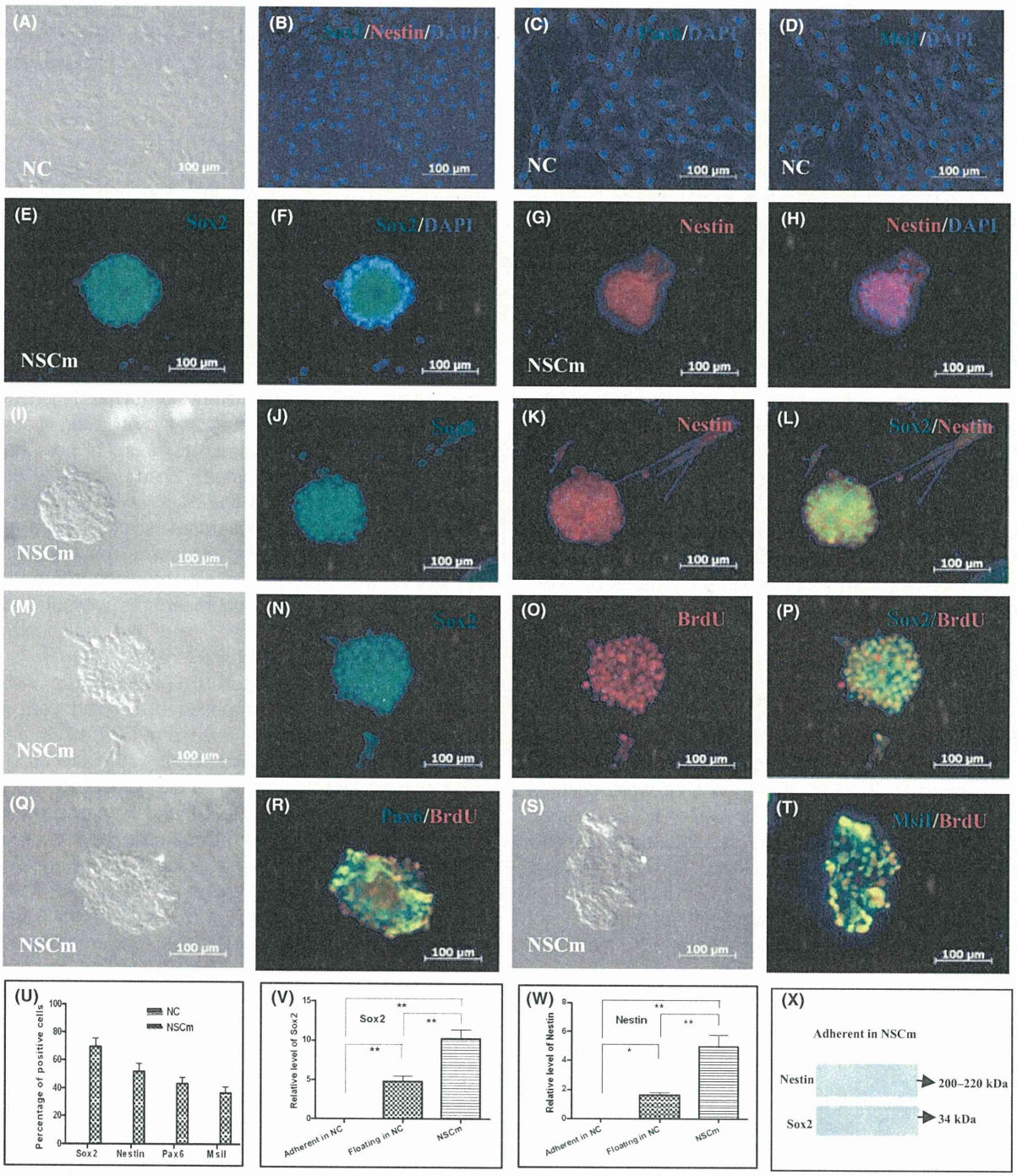

Fig. 2. Neural stem cell medium (NSCm)-cultured NIH/3T3-derived neurosphere-like cells expressed neural progenitor markers. NC-cultured NIH/3T3 fibroblasts did not express any neural progenitor marker (B–D). Single and double staining of Sox2 (E, F, J and L) and Nestin (G, H, K and L) demonstrated that these spheres co-expressed multiple neural progenitor markers. Some spheres were positively stained with BrdU and Sox2 (N-P), Pax-6 (R), Msi1 (T), indicating their proliferative property. Phase contrast images of NIH/3T3 cells cultured in NC (A) and NSCm (I, M, Q and S) were also shown. The percentage of positive cells is presented in the graph (U). Real-time PCR analysis of Sox2 (V) and Nestin (W) were performed for NIH/3T3 cells adherent in NC, floating in NC or NSCm. The columns represent the relative expression level of Sox2 or Nestin in spheres compared with those of adherent NIH/3T3 fibroblasts. Western blotting analysis of Sox2 and Nestin in NC- and NSCm-cultured NIH/3T3 cells were shown in X. The symbols * and ** represent $P < 0.05$ and $P < 0.01$, respectively.

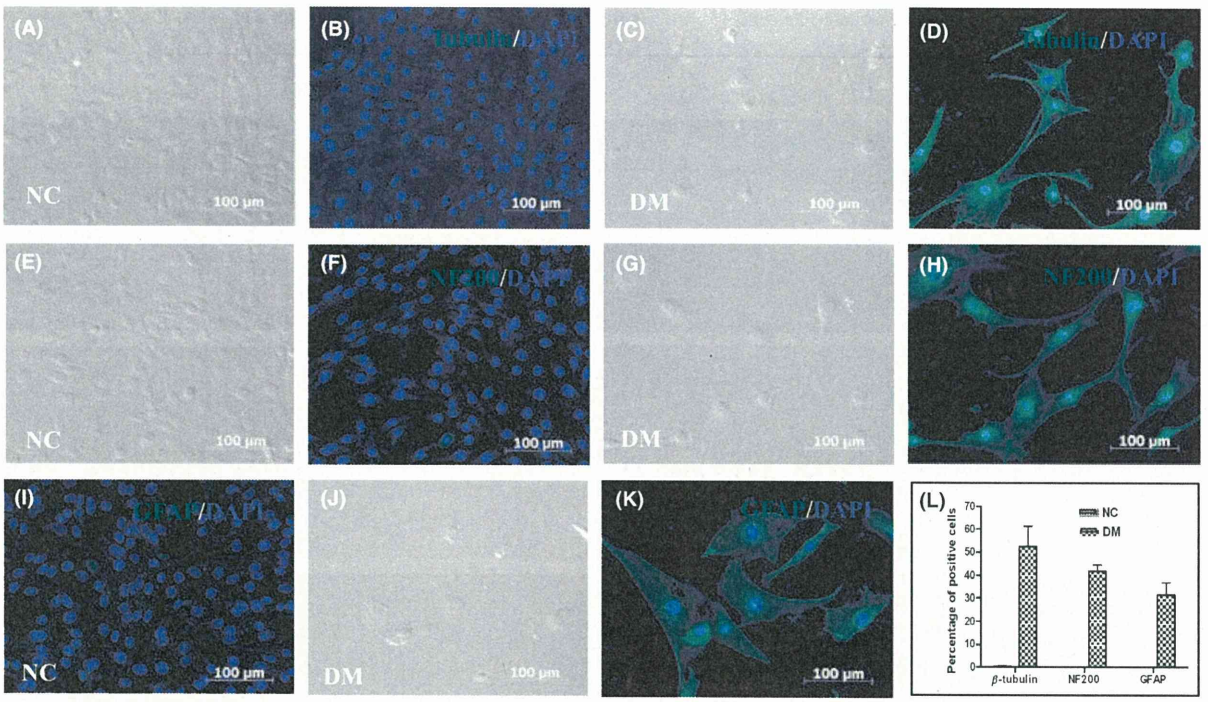

Fig. 3. Differentiation of neural stem cell medium (NSCm)-cultured NIH/3T3-derived neurosphere-like cells into neuron- and astrocyte-like cells. When shifted to DM, these cells expressed markers corresponding to neurons (β-tubulin [D] and NF200 [H]) and astrocytes (glial fibrillary acidic protein [GFAP] [K]). NIH/3T3 fibroblasts cultured in normal conditions (NC) were used as a control (A, B, E, F, and I). Phase contrast images of NIH/3T3 cells cultured in NC (A and E) and DM (C, G and J) were also shown. The percentage of positive cells expressing neuronal or glial markers is presented in the graph (L).

property is self-renewal wherein cells from spheres proliferate and make identical copies of themselves. The second is multipotency, wherein the spheres are able to generate all three main cell lineages of the mammalian central nervous system (CNS), neurons, astrocytes, and oligodendrocytes. The third is the ability to generate tissues. The generation of a neurosphere even from a particular region of the CNS does not necessarily denote to be neural progenitors unless there is supporting *in vivo* evidence (Chojnacki & Weiss 2008; Ahmed 2009). This neurosphere protocol has been used in a number of studies to examine the properties of various progenitors (Chaichana *et al.* 2006; Das *et al.* 2006; Jensen & Parmar 2006; Marshall *et al.* 2006; Chojnacki & Weiss 2008).

In the present study, we demonstrated the self-renewal property of NIH/3T3-derived spheres, and we also showed the potential of these cells to differentiate along two basic CNS lineages, neurons and astrocytes; however, we failed to show the expression of the oligodendrocyte marker O4.

These results predicted two possibilities. One is that these NIH/3T3-derived spheres are not neural progenitors, but only some NIH/3T3 cells with changes in morphology and properties. Because the growth of cells *in vivo* and *in vitro* are tightly regulated by their microenvironments (Hegde *et al.* 2007), NIH/3T3 fibroblasts are likely to survive in NSCm, display classic morphology of neurospheres and respond to growth factor exposure in a similar manner that was exhibited by neural progenitors. For example, the markers of neural progenitors were upregulated and some cells had the potential to differentiate toward neural lineage. However, most of these cells still preserved the property of NIH/3T3 fibroblasts, and could not be differentiated into all three main types of CNS lineages.

The other possibility is that these NIH/3T3-derived spheres may be immature neural progenitors. These spheres could proliferate, express markers of neural progenitors and generate neuron and astrocyte markers. The reason why these spheres did not express the oligodendrocyte marker O4 may be due to the lack of some growth factor(s) in the differentiating medium or the shortage of culture period, which may be critical for the generation of oligodendrocyte progenitors or oligodendrocytes. The cytokine CNTF alone might not be sufficient for the generation of oligodendrocytes, further investigations are needed to detect whether oligodendrocytes can be generated by adding other candidate factor(s), for example, platelet-derived

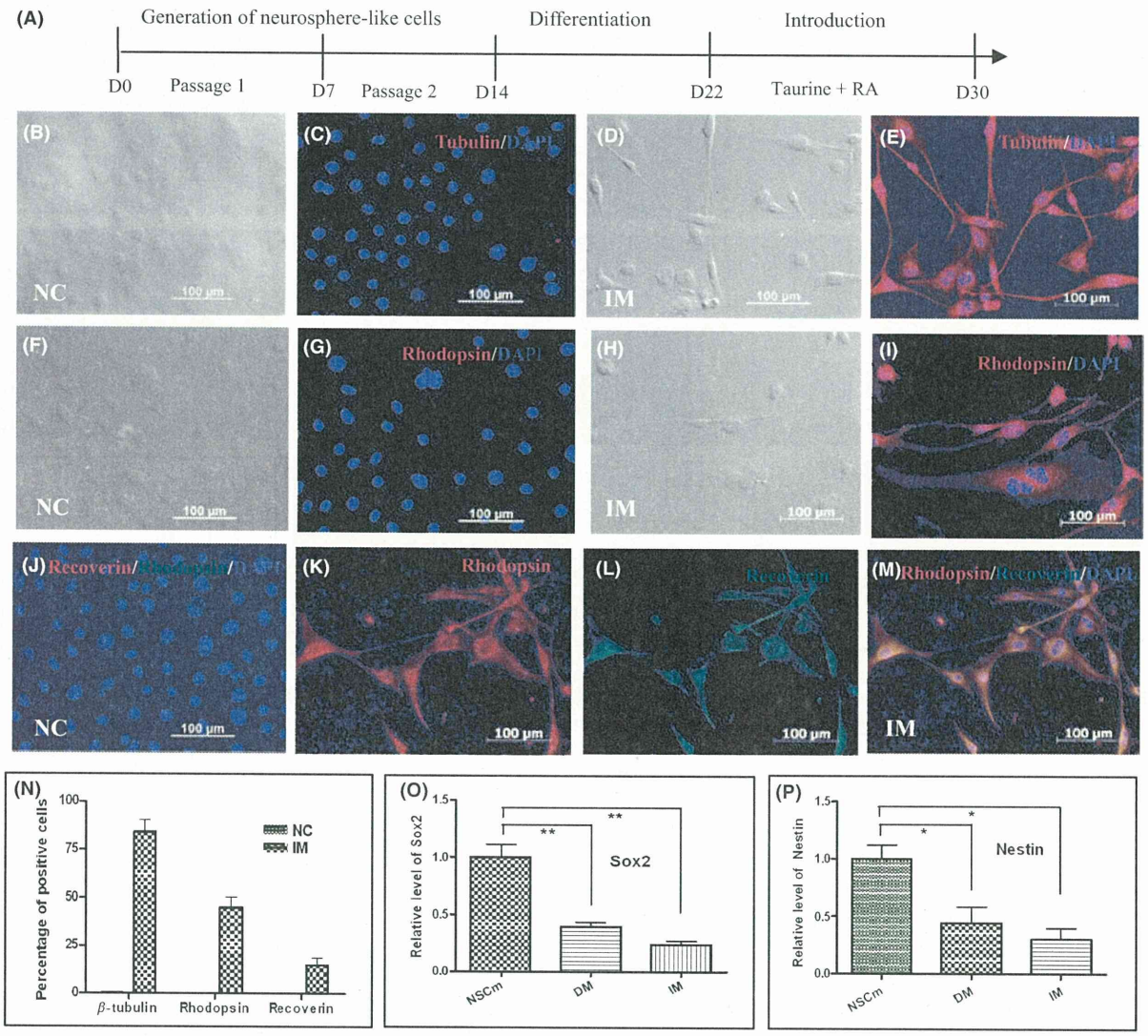

Fig. 4. Induction of neuron- and photoreceptor-like cells by treating cells with the combination of 50 μmol/L taurine and 10 μmol/L retinoic acid (RA). (A). Procedure for induction of retinal photoreceptor-like cells from NIH/3T3 fibroblasts. Immunocytochemical analysis of β-tubulin (C and E), rhodopsin (G, I, J, K and M) and recoverin (J, L and M) was performed for the treated (E, I, and K-M) and untreated (C, G and J) cells. Phase contrast images of NIH/3T3 cells cultured in NC (B and F) and IM (D and H) were also shown. The percentage of positive cells expressing neuronal or photoreceptor markers is presented in the graph (N). Real-time PCR was carried out to analyze Sox2 (O) and Nestin (P) expression in NSCm-, DM- and IM-cultured cells. The symbols * and ** represent $P < 0.05$ and $P < 0.01$, respectively.

growth factor AA, which was demonstrated to effectively enhance survival of oligodendrocyte progenitors (Yang *et al.* 2005; Chen *et al.* 2007).

Our study demonstrates that NIH/3T3 fibroblasts display some features of neural progenitors and express neuron, astrocyte and even photoreceptor markers under defined conditions. These results shed some light on the induction of retinal photoreceptors from a differentiated cell source. Further studies are necessary to determine if NIH/3T3 fibroblasts can be differentiated into functional neurons or photoreceptors, but the present study suggests that neuronal cells can be generated from differentiated cells of other types without the need of adding any epigenetic modifier.

Acknowledgments

This work was supported in part by the Ministry of Health, Labour and Welfare, Japan Foundation for Aging and Health and the Program for Promotion of Fundamental studies in Health Sciences of the National Institute of Biomedical Innovation (NIBIO).

References

Ahmed, S. 2009. The culture of neural stem cells. *J. Cell. Biochem.* **106**, 1–6.

Brewer, G. J. & Torricelli, J. R. 2007. Isolation and culture of adult neurons and neurospheres. *Nat. Protoc.* **2**, 1490–1498.

Chaichana, K., Zamora-Berridi, G., Camara-Quintana, J. & Quinones-Hinojosa, A. 2006. Neurosphere assays: growth factors and hormone differences in tumor and nontumor studies. *Stem cells* **24**, 2851–2857.

Chen, Y., Balasubramaniyan, V., Peng, J., Hurlock, E. C., Tallquist, M., Li, J. & Lu, Q. R. 2007. Isolation and culture of rat and mouse oligodendrocyte precursor cells. *Nat. Protoc.* **2**, 1044–1051.

Chojnacki, A. & Weiss, S. 2008. Production of neurons, astrocytes and oligodendrocytes from mammalian CNS stem cells. *Nat. Protoc.* **3**, 935–940.

Das, A. V., Mallya, K. B., Zhao, X., Ahmad, F., Bhattacharya, S., Thoreson, W. B., Hegde, G. V. & Ahmad, I. 2006. Neural stem cell properties of Müller glia in the mammalian retina: regulation by Notch and Wnt signaling. *Dev. Biol.* **299**, 283–302.

Hegde, G. V., James, J., Das, A. V., Zhao, X., Bhattacharya, S. & Ahmad, I. 2007. Characterization of early retinal progenitor microenvironment: presence of activities selective for the differentiation of retinal ganglion cells and maintenance of progenitors. *Exp. Eye Res.* **84**, 577–590.

Hirami, Y., Osakada, F., Takahashi, K., Okita, K., Yamanaka, S., Ikeda, H., Yoshimura, N. & Takahashi, M. 2009. Generation of retinal cells from mouse and human induced pluripotent stem cells. *Neurosci. Lett.* **458**, 126–131.

Hoffman, L. M. & Carpenter, M. K. 2005. Characterization and culture of human embryonic stem cells. *Nat. Biotechnol.* **23**, 699–708.

Holden, C. & Vogel, G. 2008. A seismic shift for stem cell research. *Science* **319**, 560–563.

Ikeda, H., Osakada, F., Watanabe, K., Mizuseki, K., Haraguchi, T., Miyoshi, H., Kamiya, D., Honda, Y., Sasai, N., Yoshimura, N., Takahashi, M. & Sasai, Y. 2005. Generation of Rx+/Pax6 + neural retinal precursors from embryonic stem cells. *Proc. Natl Acad. Sci. USA* **102**, 11331–11336.

Jensen, J. B. & Parmar, M. 2006. Strengths and limitations of the neurosphere culture system. *Mol. Neurobiol.* **34**, 153–161.

Jin, W., Xing, Y. Q. & Yang, A. H. 2009. Epidermal growth factor promotes the differentiation of stem cells derived from human umbilical cord blood into neuron-like cells via taurine induction in vitro. *In Vitro Cell. Dev. Biol. Anim.* **45**, 321–327.

Klassen, H. & Reubinoff, B. 2008. Stem cells in a new light. *Nat. Biotechnol.* **26**, 187–188.

Marshall, G. P., Reynolds, B. A. & Laywell, E. D. 2006. Using the neurosphere assay to quantify neural stem cells in vivo. *Curr. Pharm. Biotechnol.* **8**, 141–145.

Matsuda, N., Lu, H., Fukata, Y., Noritake, J., Gao, H. F., Mukherjee, S., Nemoto, T., Fukata, M. & Poo, M. M. 2009. Differential activity-dependent secretion of brain-derived neurotrophic factor from axon and dendrite. *J. Neurosci.* **29**, 14185–14194.

Osakada, F., Ikeda, H., Sasai, Y. & Takahashi, M. 2009. Stepwise differentiation of pluripotent stem cells into retinal cells. *Nat. Protoc.* **4**, 811–824.

Osakada, F., Ikeda, H., Mandai, M., Wataya, T., Watanabe, K., Yoshimura, N., Akaike, A., Sasai, Y. & Takahashi, M. 2008. Toward the generation of rod and cone photoreceptors from mouse, monkey and human embryonic stem cells. *Nat. Biotechnol.* **26**, 215–222.

Sanchez-Ramos, J., Song, S., Cardozo-Pelaez, F., Hazzi, C., Stedeford, T., Willing, A., Freeman, T. B., Saporta, S., Janssen, W., Patel, N., Cooper, D. R. & Sanberg, P. R. 2000. Adult bone marrow stromal cells differentiate into neural cells in vitro. *Exp. Neurol.* **164**, 247–256.

Sugano, E., Tomita, H., Abe, T., Yamashita, A. & Tamai, M. 2003. Comparative study of cathepsins D and S in rat IPE and RPE cells. *Exp. Eye Res.* **77**, 203–209.

Sugano, E., Tomita, H., Ishiguro, S., Abe, T. & Tamai, M. 2005. Establishment of effective methods for transducing genes into iris pigment epithelial cells by using adeno-associated virus type 2. *Invest. Ophthalmol. Vis. Sci.* **46**, 3341–3348.

Takahashi, K. & Yamanaka, S. 2006. Induction of pluripotent stem cells from mouse embryonic and adult fibroblast cultures by defined factors. *Cell* **126**, 663–676.

Woodbury, D., Schwarz, E. J., Prockop, D. J. & Black, I. B. 2000. Adult rat and human bone marrow stromal cells differentiate into neurons. *J. Neurosci. Res.* **61**, 364–370.

Yamanaka, S. 2007. Strategies and new developments in the generation of patient-specific pluripotent stem cells. *Cell Stem Cell* **1**, 39–49.

Yamanaka, S. 2009. A fresh look at iPS cells. *Cell* **137**, 13–17.

Yang, Z. S., Watanabe, M. & Nishiyama, A. 2005. Optimization of oligodendrocyte progenitor cell culture method for enhanced survival. *J. Neurosci. Methods* **149**, 50–56.

Zhang, X. M., Li, Q. M., Su, D. J., Wang, N., Shan, Z. Y., Jin, L. H. & Lei, L. 2010. RA induces the neural-like cells generated from epigenetic modified NIH/3T3 cells. *Mol. Biol. Rep.* **37**, 1197–1202.

Zhao, X., Liu, J. N. & Ahmad, I. 2002. Differentiation of embryonic stem cells into retinal neurons. *Biochem. Biophys. Res. Commun.* **297**, 177–184.

Zhou, H., Wu, S., Joo, J. Y., Zhu, S., Han, D. W., Lin, T., Trauger, S., Bien, G., Yao, S., Zhu, Y., Siuzdak, G., Schöler, H. R., Duan, L. & Ding, S. 2009. Generation of induced pluripotent stem cells using recombinant proteins. *Cell Stem Cell* **4**, 381–384.

Neuroscience Research 69 (2011) 223–233

Contents lists available at ScienceDirect

Neuroscience Research

journal homepage: www.elsevier.com/locate/neures

Lineage analysis of newly generated neurons in organotypic culture of rat hippocampus

Jun Yokose[a,b,c], Toru Ishizuka[a,b], Takeshi Yoshida[d], Jun Aoki[d], Yoshio Koyanagi[d], Hiromu Yawo[a,b,c,e,*]

[a] Department of Developmental Biology and Neuroscience, Tohoku University Graduate School of Life Sciences, Sendai 980-8577, Japan
[b] JST, CREST, Tokyo 102-0075, Japan
[c] Tohoku University Basic and Translational Research Center for Global Brain Science, Sendai 980-8575, Japan
[d] Laboratory of Viral Pathogenesis, Institute for Virus Research, Kyoto University, Kyoto 606-8507, Japan
[e] Center for Neuroscience, Tohoku University Graduate School of Medicine, Sendai 980-8575, Japan

ARTICLE INFO

Article history:
Received 16 August 2010
Received in revised form 8 November 2010
Accepted 26 November 2010
Available online 8 December 2010

Keywords:
Postnatal neurogenesis
Hippocampus
Slice culture
Retrovirus
Lineage
Differentiation
Programmed cell death
Critical period

ABSTRACT

New neurons are continuously generated in the hippocampus at the subgranular zone of the dentate granule cell layer throughout life. However, the lineage of newly generated neurons is unknown in detail. Here, using a retrovirus vector encoding EGFP, we labeled proliferating cells in an organotypic slice culture of the postnatal hippocampus of rat, and tracked their descendents over a long period. At 28 days post-inoculation, the phenotypes of the cells were immunohistochemically identified using specific antibodies to cell-type markers such as HuC/D (pan-neuronal marker), GFAP (astrocyte marker), Prox1 (dentate granule cell marker) or NeuN (mature neuronal marker). We found that the cells were mostly GFAP-negative in the HuC/D-positive lineages. The EGFP-expressing cells were often untraceable shortly after cell division in the HuC/D-positive lineages. The postmitotic periods of these cells distributed between 2 and 14 days. For the lineages expressing both Prox1 and NeuN the newborn cells became untraceable in a similar period (2–10 days). It is suggested that the newly generated neurons differentiate to mature dentate granule cells in the slice culture once they have survived over this critical traceability period.

1. Introduction

New neurons are continuously generated postnatally in the hippocampus of mammals including humans (Altman and Das, 1965; Cameron et al., 1993; Eriksson et al., 1998). When the new neurons generated in the subgranular zone (SGZ) of the dentate gyrus differentiate into functional dentate granule cell layer (GCL) neurons, they are integrated into the hippocampal circuitry for certain forms of memory such as spatial relation memory and/or contextual fear conditioning, although some findings remain controversial (Bruel-Jungerman et al., 2006; Meshi et al., 2006; Saxe et al., 2006; Dupret et al., 2008; Imayoshi et al., 2008; Zhang et al., 2008; see reviews by Aimone et al., 2006; Lledo et al., 2006; Kempermann, 2008). In the postnatal hippocampus, neurogenesis is a multi-step process consisting of the division of a putative stem/precursor cell (type-1 cell), the transient amplification of putative progenitor cells (type-2, -3 cells), the selection of surviving cells and their differentiation into functional neurons (Kempermann et al., 2004). The stem cells could be multi-potent with the ability to generate neurons, astrocytes and oligodendrocytes (Palmer et al., 1997). On the other hand, the type-2, -3 cells are thought to be destined to generate neurons since these cells are positive for immature neuronal marker proteins such as doublecortin and PSA-NCAM as well as for membrane properties reminiscent of immature neurons (Brown et al., 2003; Fukuda et al., 2003; Filippov et al., 2003; Kronenberg et al., 2003). The multi-potent precursor cells transform to the neuron-destined cells early during the type-2 cell stage (Steiner et al., 2006). Every step has been presumed to be under the regulation of various neurogenic stimuli. For example, voluntary movements such as the wheel running, facilitate the proliferation of transiently amplifying progenitor cells, whereas environmental enrichment may facilitate the survival of the final descendents (Kempermann et al., 1997; van Praag et al., 1999; Kronenberg et al., 2003; Bruel-Jungerman et al., 2005; Steiner et al., 2006, 2008). To further investigate how the proliferation and the survival are regulated, the lineage has to be followed up for an individual progenitor

Abbreviations: DIV, days *in vitro*; DPI, days post-inoculation; RV, retrovirus vector.

* Corresponding author at: Department of Developmental Biology and Neuroscience, Tohoku University Graduate School of Life Sciences, 2-1-1 Katahira, Aoba-ku, Sendai 980-8577, Japan. Tel.: +81 22 217 6208; fax: +81 22 217 6211.
E-mail addresses: a9bd2009@s.tohoku.ac.jp (J. Yokose), ishizuka@m.tohoku.ac.jp (T. Ishizuka), koegadekaina@ybb.ne.jp (T. Yoshida), quizmaster0918@yahoo.co.jp (J. Aoki), ykoyanag@virus.kyoto-u.ac.jp (Y. Koyanagi), yawo-hiromu@m.tohoku.ac.jp (H. Yawo).

0168-0102/$ – see front matter © 2010 Elsevier Ireland Ltd and the Japan Neuroscience Society. All rights reserved.
doi:10.1016/j.neures.2010.11.010

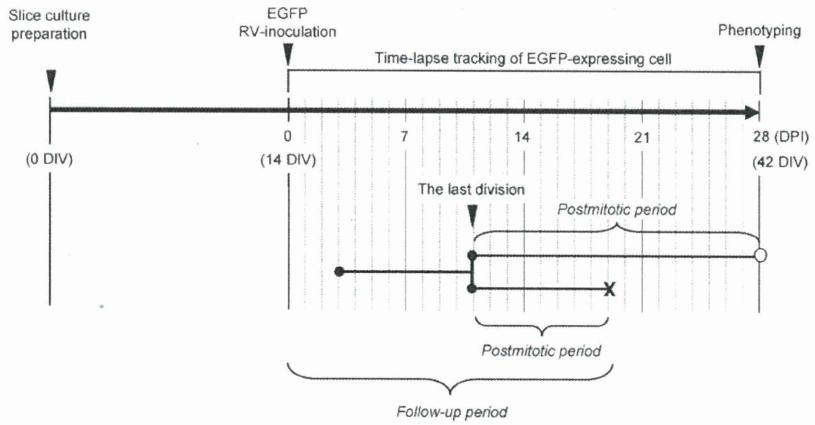

Fig. 1. Experimental protocol of lineage analysis. The newly generated cells and their descendents were followed after the inoculation of the retrovirus vector (RV) encoding EGFP. Their phenotypes were determined immunohistochemically at 28 days post-inoculation (DPI). The follow-up period was measured from the date of retrovirus vector inoculation in DPI. The postmitotic period was measured from the last division to the time of interest.

cell since the onset of each key process of neurogenesis occurs asynchronously.

Although the neurogenic processes have been extensively studied using animal model systems *in vivo*, it appears to be difficult to identify a single progenitor cell and to track its fate for a certain period. To solve this, here we used the organotypic slice culture of hippocampus as an *ex vivo* model preparation (Kamada et al., 2004; Raineteau et al., 2004; Laskowski et al., 2005; Poulsen et al., 2005). In the slice culture, the network is organized similar to that in living animals (Gähwiler, 1984; Zimmer and Gähwiler, 1984; Dailey et al., 1994) with a few rearrangements as a consequence of the afferent deprivation (Robain et al., 1994; Gutierrez and Heinemann, 1999) and the morphological and the physiological features of a neuron are similar to those in living animals (Stoppini et al., 1991; Okada et al., 1995; Gähwiler et al., 1997). Moreover, the newly generated cells can be directly observed under fluorescent microscopy (Kamada et al., 2004; Namba et al., 2007). In the present study, using retrovirus vectors, we labeled the newly generated cells with EGFP, investigated the lineage of individual progenitors for up to four weeks in the hippocampal slice culture and identified their phenotypes using HuC/D as a molecular marker of the neuron-generating lineage. The slice culture system enabled us to track a single progenitor cell and its descendents as a lineage in the postnatal hippocampus. Furthermore, the results indicate that the cells became often untraceable 2–14 days after cell division in the neuron-generating lineages.

2. Materials and methods

All animal experiments were approved by the Tohoku University Committee for Animal Experiments and were carried out in accordance with the Guidelines for Animal Experiments and Related Activities in Tohoku University as well as the guiding principles of the Physiological Society of Japan and the NIH.

2.1. Hippocampal slice culture

Hippocampal organotypic cultures were prepared from postnatal day 7 (P7) Wistar rats (Japan SLC Inc., Shizuoka, Japan) and cultured according to the standard interface method with some modifications (Stoppini et al., 1991; Sakaguchi et al., 1994; Kamada et al., 2004). Briefly, after decapitation the brain was removed, dissected and transversely sliced at the hippocampus into a 350 μm thickness on a McIlwain tissue chopper (The Mickle Laboratory Engineering, Guildford, Surrey, UK). In our experiments, slices were usually obtained from the dorsal part of rat hippocampus. The isolated slices were incubated on ice for at least 15–20 min in a solution containing (in mM) 236 mannitol, 3 KCl, 10 HEPES, 4 NaOH, 7 $MgCl_2$, 22 D-glucose, 1 kinurenic acid, penicillin and streptomycin (100 U/ml and 100 μg/ml, respectively), and were transferred onto porous membrane inserts (Millicell-CM: PICM03050, Millipore, Billerica, MA, USA). The slices were maintained in a humidified incubator at 34 °C in a 5% CO_2 atmosphere. The culture medium consisted of 50% OPTI-MEM (Invitrogen, Carlsbad, CA, USA), 25% heat-inactivated horse serum (Invitrogen) and 25% Hank's balanced salt solution (Invitrogen). It was further supplemented with D-glucose (5 g/L), penicillin (100 U/ml, Sigma–Aldrich, St. Louis, MO, USA) and streptomycin (100 μg/ml, Sigma–Aldrich), and was changed twice a week.

2.2. Retrovirus inoculation and time-lapse tracking of EGFP-expressing cells

Retroviral vectors encoding EGFP were prepared as described previously (Kamada et al., 2004) and their titers were 9×10^6 transduction U/ml. We reduced the amount of virus solution as little as possible so as the EGFP-expressing cells to be found in isolation. Typically, 0.1–0.2 μl of the solution containing these vectors was injected by at three positions in the suprapyramidal blade of the GCL in slices at 14 days *in vitro* (14 DIV), and the injected sites in the suprapyramidal region were daily observed (Fig. 1) under an inverted fluorescent microscope (Axiovert 200, Carl Zeiss, Göttingen, Germany) equipped with a 32× objective with long working distance (32×, LD A-Plan, Carl Zeiss). As only proliferating cells incorporate the transgene into their genome by the retroviral labeling method, newly generated cells and their descendants would specifically express EGFP. Once the EGFP-expressing cell was found in isolation, it was centered to the visual field and imaged at every two days for up to 28 days post-inoculation (28 DPI). The change of the visual field was kept to minimum during the tracking period by using several other fluorescent cells as landmarks. To prevent alkalization of the medium, the slices were kept in a humidified 5% CO_2/95% O_2 environment during imaging on the microscope. When the image clearly indicated division of the targeted cell, it was defined as the date of cell division. When a tracked cell was not found anywhere from top to bottom of the slice in the monitoring region (width ±295 μm; height ±394 μm) of the dentate gyrus, the cell was defined as "untraceable" because it could not be proven as having died. The first day of this detection was defined as the date of untraceability. At 28 DPI, the slices were fixed and subjected to immunohistochemistry as described below. Each new-

born cell and its descendents were tracked up to 28 DPI, identified their phenotypes and summarized as a cell lineage.

As shown in Fig. 1, the time measured from the date of retrovirus inoculation to that of untraceability was defined as the follow-up period. The time measured from the date of last division to that of untraceability was defined as the postmitotic period. The postmitotic period of a survived cell was measured as that between the last division and the phenotyping at 28 DPI, although this would be an underestimation.

2.3. Immunohistochemistry

Phenotypes of the newly generated EGFP-expressing cells were investigated immunohistochemically at 17 DIV (3 DPI) (42 slices, 230 cells) or at 42 DIV (28 DPI) (57 slices, 110 cells) using antibodies to Nestin, GFAP, HuC/D, Plox1 and NeuN in combination. Nestin is one of the intermediate filaments expressed specifically in neuroblasts and myoblasts (Lendahl et al., 1990) and a putative neural precursor marker (Ernst and Christie, 2005; Lagace et al., 2007). GFAP is a marker of non-neuronal cells (Seri et al., 2001) including terminally differentiated astrocytes (Goldman, 2003; Seri et al., 2004), radial glial cells, which have neurogenic potential (Seri et al., 2001), and type-1 neural progenitors (Kronenberg et al., 2003; Kamada et al., 2004). Members of Hu protein family have been identified as RNA-binding proteins that are expressed in both early postmitotic and mature neurons and are involved in the differentiation and/or the maintenance of neurons (Wakamatsu and Weston, 1997; Akamatsu et al., 2005). Prox1 is specifically expressed in mature GCL neurons and immature neurons that are differentiating to them (Alfonoso and Guillermo, 2007; Galeeva et al., 2007). NeuN is a specific marker of mature neurons.

Slices were fixed with 4% paraformaldehyde in 0.1 M sodium phosphate buffer (pH 7.2) at 4 °C for 30 min and then washed in PBS. After the slices were peeled off from the membrane, all subsequent incubations were carried out in free-floating mode in a dish. The slices were blocked in PBS including 5% normal donkey serum and 0.3% Triton X-100 at 4 °C overnight, then treated with the primary antibodies in PBS including 5% donkey serum and 0.3% Triton X-100 at 4 °C for 24 h. In a series of experiments the sample was triply labeled by the combination of the following primary antibodies: rabbit anti-EGFP IgG (1:1000; a generous gift from Drs. T. Kaneko and K. Nakamura, Kyoto University, Japan), rat anti-GFP IgG (1:2000; 04404-26, Nacalai tesque, Kyoto, Japan), guinea pig anti-GFAP IgG (1:1000; 03223, Advanced Immunochemical, Long Beach, CA, USA), mouse anti-HuC/D IgG (IgG_{2b}, 1:1000; A21271, Molecular probes, Eugene, OR, USA), rabbit anti-Prox1 IgG (1:2000; AB5475, Chemicon, Tamecula, CA, USA) and mouse anti-NeuN IgG (1:1000; MAB377, Chemicon). After washing four times (30 min each) at room temperature in PBS with 0.1% Triton X-100 the slices were incubated at room temperature for 5–6 h with the following secondary antibodies in PBS including 5% normal donkey serum and 0.3% Triton X-100: Alexa Fluor 488-, 647-conjugated donkey anti-mouse IgG, Alexa Fluor 488-, 546-conjugated donkey anti-rabbit IgG, Alexa Fluor 633-conjugated goat anti-rabbit IgG, Alexa Fluor 568-, 633-conjugated goat anti-Guinea pig IgG and Alexa Fluor goat 488-conjugated anti-rat IgG (1:200; all purchased from Molecular Probes).

For the triple labeling with two mouse monoclonal antibodies, we used the Zenon mouse IgG labeling kit with either Alexa Fluor 546 (Z25004, Molecular Probes) or 647 (Z25208, Molecular Probes). Anti-Nestin IgG_1 (1:1000; MAB353, Chemicon) or anti-HuC/D IgG_{2b} (1:200) was incubated with fluorophore-labeled Fab fragments for 5 min at room temperature. The Fab fragments/primary antibody molar ratio was 6:1. The mixture was followed by blocking solution for 5 min at the same ratio and applied to the slice for 5 h at room temperature. Finally, the slices were washed four times in PBS with 0.1% Triton X-100 and mounted on glass slides with Permafluor (Beckman Coulter, Brea, CA, USA).

Each specimen was analyzed three-dimensionally with a z-axis interval of 0.84–0.87 μm under conventional confocal laser-scanning microscopy (LSM510META, Carl Zeiss) equipped with a 40× objective. All images were corrected for brightness and contrast using LSM Image Browser version 3.2 (Carl Zeiss), Photoshop version 6.0, (Adobe Systems Inc, San Jose, CA, USA) and ImageJ (http://rsbweb.nih.gov/ij/). The coexpression of phenotype markers was usually confirmed three-dimensionally under higher magnification.

2.4. Numerical and statistical analyses

The proliferation curves of newly generated cells were predicted for each type of lineage according to the following equation:

$$\text{Number of EGFP-expressing cells} = \prod_i (1 + f_i), \quad (1)$$

where f_i is the frequency of cell division during the ith period after retrovirus inoculation. The following survival probability was calculated for each lineage and was summarized.

$$\text{Survival probability} = \frac{\text{Number of cells counted at 28 DPI}}{\text{Total number of cells produced during 1 – 28 DPI}}. \quad (2)$$

All data in the text are presented as mean ± SEM (number of observation), and statistical significance was assessed using the non-parametric tests as the distribution functions were mostly unpredictable.

3. Results

3.1. Phenotypes of newly generated cells in the slice culture

The gross appearances and cellular architecture of the cultured hippocampal slices were similar to those from living animals between 14 and 42 days *in vitro* (DIV) as noted in the previous studies (Stoppini et al., 1991; Okada et al., 1995; Kamada et al., 2004). Within several days post-inoculation (DPI), EGFP-expressing cells were recognized around SGZ of the suprapyramidal blade of the GCL as shown in Fig. 2A. Under daily surveillance of the injected sites by fluorescent microscopy, round EGFP-expressing cells appeared on 2–3 DPI (Fig. 2Bi). Some of them had proliferated (Fig. 2Bii and Bviii), and migrated. Occasionally, one of the newly generated cells was untraceable (Fig. 2Bvii and Bxi) whereas the other differentiated with neuron-like morphology (Fig. 2Bxii–xiv).

Phenotypes of the newly generated EGFP-expressing cells were investigated immunohistochemically at 17 DIV (3 DPI) using two antibodies, anti-nestin and anti-GFAP (Supplementary Fig. S1A). Among the EGFP-expressing cells in the GCL (21 slices, 117 cells), 20 cells (17%) were both nestin- and GFAP-positive ($Nestin^+/GFAP^+$), 24 cells (21%) were nestin-positive but GFAP-negative ($Nestin^+/GFAP^-$), 12 cells (10%) were nestin-negative but GFAP-positive ($Nestin^-/GFAP^+$), whereas 61 cells (52%) were positive for neither ($Nestin^-/GFAP^-$) (Supplementary Fig. S2A). In another series of experiments, the phenotypes of newly generated EGFP-expressing cells were identified by the combination of anti-nestin and anti-HuC/D (Supplementary Fig. S1B). Among the EGFP-expressing cells (21 slices, 113 cells), 39 cells (35%) were both nestin- and HuC/D-positive ($Nestin^+/Hu^+$), 19 cells (17%) were nestin-positive but HuC/D-negative ($Nestin^+/Hu^-$), 19 cells (17%) were nestin-negative but HuC/D-positive ($Nestin^-/Hu^+$), whereas 36 cells (32%) were positive for neither ($Nestin^-/Hu^-$) (Supplementary Fig. S2B).

After tracking the lineage of EGFP-expressing cells their final phenotypes were identified at 42 DIV (28 DPI) using two antibodies, anti-HuC/D and anti-GFAP (Fig. 3). Among 110 cells examined

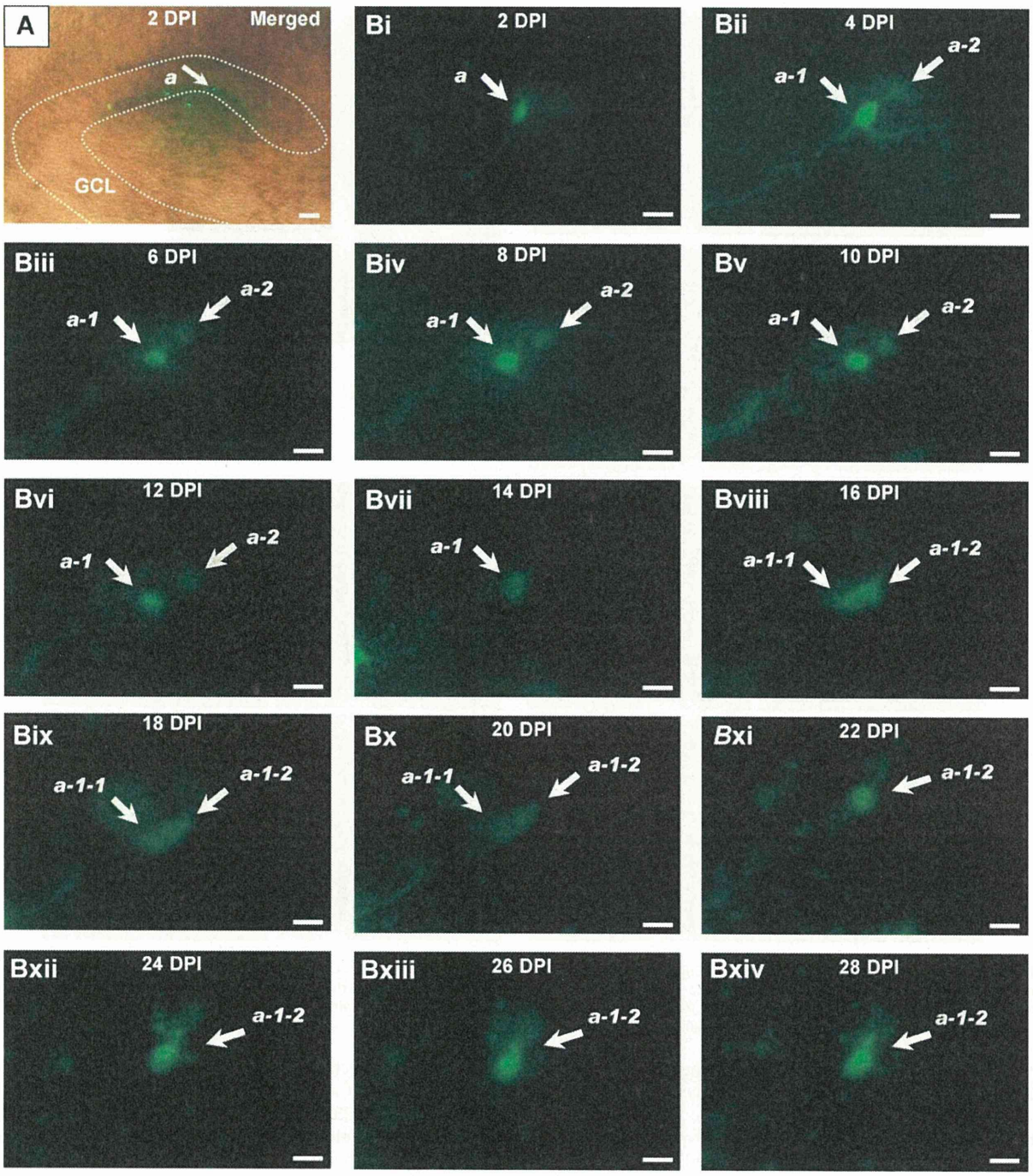

Fig. 2. Long-term survey of the newly generated cells in an organotypic culture of the hippocampus. (A) The slice culture at 2 DPI (16 DIV). The fluorescence image was overlaid on the plain picture. One of the EGFP-expressing cells (a, arrowed) was traced in Bi–ivx. GCL, the granule cell layer. (B) The daily surveillance of the fate of a newborn cell. A round EGFP-expressing cell, (a) was detected on the 2 DPI (Bi) and divided to produce a-1 and a-2 (Bii). One of them, a-2 became untraceable (Bvii) whereas another divided again to produce a-1-1 and a-1-2 (Bviii). One of them, a-1-1 became untraceable (Bxi), whereas another, a-1-2 differentiated with a neuronal morphology (Bxii–xiv). Scale bars, 100 μm in A and 20 μm in B.

(57 slices), 41 cells (37%) were HuC/D-positive but GFAP-negative ($Hu^+/GFAP^-$), 29 cells (26%) were GFAP-positive but HuC/D-negative ($Hu^-/GFAP^+$) and 40 cells (36%) were neither HuC/D- nor GFAP-positive ($Hu^-/GFAP^-$). We could not find any cells that were both HuC/D- and GFAP-positive. Therefore, according to the triple fluorescent labeling (anti-EGFP, anti-HuC/D and anti-GFAP), we classified the lineage of an EGFP-expressing cell as either "HuC/D-positive" or "GFAP-positive" groups. The cells that were negative to both HuC/D and GFAP were grouped as "unclassified". Some of the EGFP-expressing cells, which had dendrite-like processes (Fig. 3Ai), showed coexpression of HuC/D (Fig. 3Aii and B) but not GFAP (Fig. 3Aiii and Aiv). Other EGFP-positive cells with star-like appearances (Fig. 3Ci) were HuC/D-negative (Fig. 3Cii) and GFAP-positive (Fig. 3Ciii and Civ). We also found EGFP-positive, HuC/D-negative and GFAP-positive cells with the appearance of radial glia (Fig. 3Di–iv).